Geochemistry Geophysics Geosystems G3

Article
Volume 11, Number 11
12 November 2010
Q11007, doi:10.1029/2010GC003293
ISSN: 1525-2027

Published by AGU and the Geochemical Society

No slab-derived CO_2 in Mariana Trough back-arc basalts: Implications for carbon subduction and for temporary storage of CO_2 beneath slow spreading ridges

Colin G. Macpherson
Department of Earth Sciences, University of Durham, Durham DH1 3LE, UK (colin.macpherson@durham.ac.uk)

Also at Geosciences Research Division, Scripps Institution of Oceanography, University of California, San Diego, La Jolla, California 92093-0244, USA

David R. Hilton
Geosciences Research Division, Scripps Institution of Oceanography, University of California, San Diego, La Jolla, California 92093-0244, USA

Konrad Hammerschmidt
Institute of Geological Sciences, Free University Berlin, D-12249 Berlin, Germany

[1] The Southern Mariana Trough is particularly well suited to study mass balance in subduction zones because the flux of material recycled from the subducted slab has been shown to diminish to negligible levels in the southernmost part of the area. We present new He and Ar concentration and isotopic data for 16 back-arc basaltic glasses and combine these with previously published CO_2 and H_2O concentration and $\delta^{13}C$ data to explore the recycling of carbon and light noble gases in the Mariana back arc. Degassing has affected all samples and is particularly extensive in more water-rich samples, i.e., those containing the largest recycled component. The degassing history features three stages: (1) deep degassing which commenced when the melt reached saturation of CO_2 and noble gases in the mantle, (2) preeruptive degassing during storage in the crust-mantle transition zone which involved addition of extraneous CO_2 to the vapor phase, and (3) eruption. CO_2 released during stage 1 was, at least partially, incorporated into wall rock and subsequently remobilized during stage 2 degassing of later magma batches. Reconstructed parental values for $^3He/^4He$, $\delta^{13}C$, $CO_2/^3He$, and $CO_2/^{40}Ar^*$ are indistinguishable from those of mid-ocean ridge basalt. This implies that there is negligible recycling of subducted carbon, helium, or argon into the source of Mariana Trough basalt.

Components: 14,400 words, 10 figures, 2 tables.

Keywords: CO_2; noble gas; Mariana Trough; basalt; assimilation; subduction.

Index Terms: 1031 Geochemistry: Subduction zone processes (3060, 3613, 8170, 8413); 1032 Geochemistry: Mid-oceanic ridge processes (3614, 8416); 1036 Geochemistry: Magma chamber processes (3618).

Received 8 July 2010; **Revised** 14 September 2010; **Accepted** 21 September 2010; **Published** 12 November 2010.

Macpherson, C. G., D. R. Hilton, and K. Hammerschmidt (2010), No slab-derived CO_2 in Mariana Trough back-arc basalts: Implications for carbon subduction and for temporary storage of CO_2 beneath slow spreading ridges, *Geochem. Geophys. Geosyst.*, *11*, Q11007, doi:10.1029/2010GC003293.

1. Introduction

[2] Subduction transports volatile species, notably water and CO_2, from Earth's surface reservoirs (e.g., hydrosphere, biosphere, atmosphere, sediments and crust) to both the shallow and deep mantle. Subducted water, in particular, has the potential to influence the physical and chemical properties of the mantle. One obvious consequence is water-induced melting in mantle wedges and the generation of subduction-related magmas. In turn, magmatic activity at subduction zones contributes to new volatile additions to external reservoirs. Therefore, subduction recycling is a fundamental means of adding volatiles back from the mantle to Earth's surface. In the case of carbon, this process has helped generate and maintain the exosphere and, so, support life [*Ridgwell and Zeebe*, 2005; *Hayes and Waldbauer*, 2006; *Hirschmann and Dasgupta*, 2009].

[3] The extent to which any single volatile species can use the subducting slab as a vehicle for recycling back to the surface (via the fore arc, the arc front, or back arc) versus continued transport to the deeper mantle depends on where and when mobilization from the slab occurs. Consequently, numerous studies have attempted to characterize the stability of volatile-bearing species under different P-T conditions which represent slabs at various stages and conditions of subduction. In the case of carbon, *Kerrick and Connelly* [2001], *Dasgupta et al.* [2004], and *Gorman et al.* [2006] have all modeled release from, or retention within, the slab, from the earliest stage of the slab entering the trench to beyond the zone of arc magma production and hence the deeper mantle. One obvious means to test the validity of this approach is through direct observation of carbon outputs at modern subduction zones [e.g., *Garcia et al.*, 1979; *Mattey et al.*, 1984; *Hilton et al.*, 1993, 2002; *Macpherson and Mattey*, 1994; *Sano and Marty*, 1995; *Ikeda et al.*, 1998; *Nishio et al.*, 1998; *Sano et al.*, 1998; *Newman et al.*, 2000; *Shaw et al.*, 2004; *Wallace*, 2005]. However, a major caveat is the assumption that point source measurements of carbon discharge, at individual regions of egress such as volcanoes, are necessarily representative of fluxes from the subducted slab [e.g., *Hilton et al.*, 2007]. Furthermore, the low and different solubilities of many volatiles in basaltic melt, which carries volatiles from the mantle wedge to the arc lithosphere, means that the abundances of volatile species relative to one another are potentially susceptible to fractionations during transport from the slab to the sampling site.

[4] In this study, we present new abundance and isotopic data for helium and argon in back-arc basaltic glasses of the Southern Mariana Trough. These results are combined with published CO_2 and H_2O abundances and $\delta^{13}C$ values [*Macpherson et al.*, 1999; *Newman et al.*, 2000] to assess the flux of slab-derived carbon. This is achieved through new modeling of volatile evolution in both the dissolved and vapor components of the magmas. The Southern Mariana Trough glasses are particularly well suited because prior study of lithophile elements demonstrates that the magnitude of the recycled flux diminishes in a systematic fashion to negligible amounts in the south [*Gribble et al.*, 1996]. This observation provides an important step toward constraining the volatile mass balance for a cold subduction zone, and reveals how magma experiences a complex sequence of degassing, wall rock carbonation and interaction with wall rock as it is emplaced through a slow spreading ridge system. These results have clear implications for understanding the carbon volatile cycle in the Marianas system and in other subduction zones.

2. Geological Setting and Samples

[5] The Mariana Trough back-arc basin is the result of arc-normal extension, between 13° and 23°N, behind the Mariana Arc in the western Pacific (Figure 1). Extension occurs by seafloor spreading in the central trough and by rifting toward the north, where the locus of extension approaches the arc [*Gribble et al.*, 1998]. Accompanying this northward change in extensional style, Mariana lavas display increases in (1) water concentrations, (2) mean degrees of partial melting, and (3) trace element and isotopic evidence of recycling from the subducted slab [*Gribble et al.*, 1996, 1998; *Newman et al.*, 2000; *Pearce et al.*, 2005]. As a result, the Mariana Trough has produced a spectrum of compositions from close to mid-ocean ridge basalt (MORB), around 15°N, to arc-like lavas where the zone of extension converges with the arc.

[6] The Southern Mariana Trough possesses ridge morphology, comprising an axial valley with inward facing normal faults and a series of axial volcanic ridges (Figure 1 [*Stüben et al.*, 1998]). This suggests a slow spreading ridge, which is consistent with spreading rate determinations at 18°N, which range between 15 and 22 mm/a [*Bibee et al.*, 1980; *Gribble et al.*, 1996; *Stüben et al.*, 1998, and references therein]. Between 15° to 17°N the trough can be split into southern and northern zones based on ridge

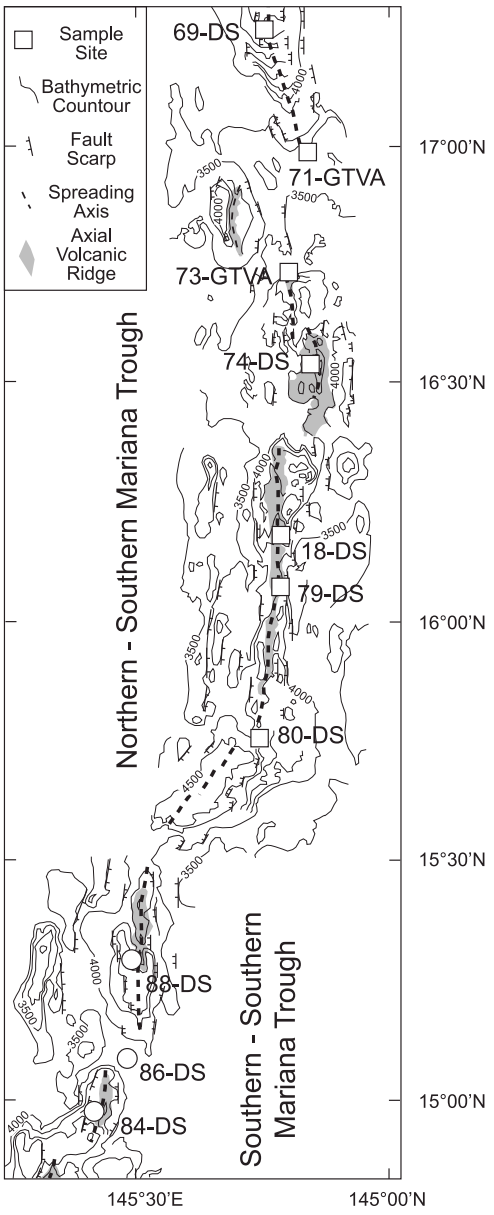

Figure 1. Map of the Southern Mariana Trough showing locations of sample sites included in this study. Depths on bathymetric contours are given in meters below sea level. Modified after *Stüben et al.* [1998].

morphology, crustal thickness and basalt composition [*Gribble et al.*, 1996; *Stüben et al.*, 1998; *Kitada et al.*, 2006]. The southern section of the Southern Mariana Trough (S-SMT) erupts olivine tholeiites and alkali basalts that reflect relatively low degrees of partial melting and a low input from the subducting slab. North of 15.5°N the ridge shoals to become the northern section of the Southern Mariana Trough (N-SMT). The olivine and quartz tholeiites erupted here carry a greater input from the subducted slab than the S-SMT [*Gribble et al.*, 1996]. This distinction is well illustrated by variations in H_2O and Ce (Figure 2). The H_2O/Ce ratio of basaltic magma is modified little by partial melting or fractional crystallization because the compatibilities of H_2O and Ce are similar in basaltic melt [*Michael*, 1995]. Therefore, H_2O/Ce provides a valuable proxy for water content in the mantle from which basaltic melt was extracted. H_2O/Ce ratios of the southernmost S-SMT tholeiites and alkali basalt are similar to MORB (Figure 2). Close to 15.5°N the ratios are greater than MORB reflecting a water-rich source. In N-SMT tholeiites, the ratios are significantly higher than MORB, a feature shared with primitive lavas from other subduction zones [*Plank et al.*, 2009]. Elevated H_2O contents in the N-SMT mantle result from a greater influx of water released by the subducted Pacific Plate as the distance between the axis of spreading and the arc diminishes [*Gribble et al.*, 1998]. More extensive mantle hydration is also responsible for the higher degrees of partial melting toward the north [*Stolper and Newman*, 1994; *Gribble et al.*, 1996, 1998; *Macpherson et al.*, 2000; *Newman et al.*, 2000; *Pearce et al.*, 2005].

[7] This study presents new vesicle and glass matrix He and Ar data for a suite of SMT basaltic glasses that includes olivine tholeiites and an alkali basalt (DS86-4-2) from the S-SMT and olivine and quartz tholeiites from the N-SMT. *Gribble et al.* [1996] presented and discussed the petrology and major element, trace element and lithophile isotope geochemistry of these glasses. The analysis of CO_2 and H_2O concentrations in these glasses, and their distribution between vesicles and glass matrix, is reported by *Macpherson et al.* [1999] and *Newman et al.* [2000]. In this contribution we integrate all volatile data for SMT magmatism.

3. Analytical Methods

[8] Samples, which were collected during cruise 69 of the R/V *Sonne* [*Gribble et al.*, 1996], were crushed using a stainless steel pestle and mortar so that fresh glass chips and shards could be selected by hand picking under a binocular microscope. Glasses were then cleaned ultrasonically in acetone and double-distilled water to remove any adhering matrix and/or alteration phases. A final picking procedure ensured that only glass pieces (mostly 1 to 5 mm in diameter) with either completely vitreous surfaces or no visible signs of alteration were selected for analysis. Analyses were conducted on three or four

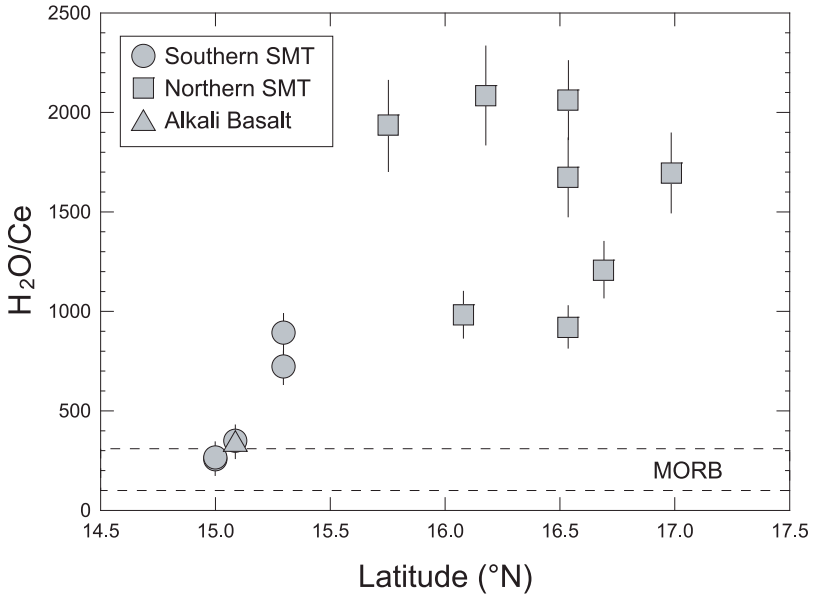

Figure 2. H_2O/Ce versus latitude for Southern Mariana Trough (SMT) basaltic glasses. H_2O/Ce calculated using Ce data of *Gribble et al.* [1996] and water concentrations from this study and *Newman et al.* [2000]. The dashed lines show the range of values for mid-ocean ridge basalt (MORB) from *Michael* [1995] and *Dixon et al.* [2002].

separate splits of each glass; one for CO_2 and water, one (or two) for helium and one for argon, to resolve the dissolved (glass-sited) and vapor (vesicle-sited) components of each gas for every sample.

[9] CO_2 and H_2O concentrations in SMT glasses were determined by heating in 100°C steps from 400° to 1200°C. This allowed sequential recovery of, first, surface contaminants (400° and 600°C), then vesicle CO_2 (700° to 900°C), and finally dissolved CO_2 (>900°C). *Macpherson et al.* [1999] present a comprehensive discussion of this and of $\delta^{13}C$ measurement of CO_2. H_2O, which is dominantly a dissolved component, recovered during the 600° to 1200°C steps of the same experiments was pooled then reduced over Zn to H_2 for peak height analysis in a gas source mass spectrometer [*Macpherson et al.*, 2005a].

[10] A brief outline of helium and argon analyses is presented below but more detail is given by *Hilton et al.* [1993]. Helium was released from glass by crushing in vacuum and by total fusion of glass chips and/or the powdered residues of crushing. Crushing released the vapor gas. Where it could be recovered, residual glass powder after crushing was fused (powder melts) to determine the dissolved He component in the crushed split. In other cases, we fused a separate split of whole glass chips to calculate the composition of the dissolved He by mass balance between this whole-rock melt and the crush experiment. Total blanks for crushing and melting procedures are identical within error at 1.5 (±1.0) × 10^{-10} cm^3 STP ^4He with atmospheric $^3He/^4He$ ratio. $^3He/^4He$ isotope ratios were determined using a MAP 215E noble gas mass spectrometer.

[11] Following a 130°C preheat for 24 h, Ar analysis by stepped heating removed adsorbed surface contamination at 400°C then sequentially extracted vesicle and dissolved components at 800°C and 1200°C, respectively [*Hilton et al.*, 1993; *Shaw et al.*, 2004; *Macpherson et al.*, 2005a]. Each 25 min step was followed by a total fusion to purge the furnace and residue. Argon isotopic analyses were conducted using an in-house fabricated, 15 cm radius, 60″ magnetic sector mass spectrometer [*Hammerschmidt*, 1986]. All mass/charge ratios between 35 and 44 were monitored, with peaks 36 to 40 extrapolated to the time of gas inlet for calculation of the relevant ratios. Peak switching was achieved by automated adjustment of the accelerating voltage. Argon sensitivity was determined by measuring known volumes of argon standards that were processed and analyzed under identical conditions to samples. Blanks, run after each sample, were typically 2.5 to 4.1 × 10^{-9} cm^3 STP ^{40}Ar between temperatures 500 to 1200°C, and generally a factor 2 to 4 higher for the fusion step. The $^{40}Ar/^{36}Ar$

Table 1. He and Ar Concentrations and Isotopic Ratios of Southern Mariana Trough Basaltic Glasses

	Southern SMT					Northern SMT										
	84-3-1	86-4-2	86-6	88-1-1	88-1-4	80-5-1	79-2-1	18-1-3	74-1-1	74-2-4	74-3-2	74-5-1	73-1-2	71-1-1	71-3	69-1-2
Crush[a]																
[^{4}He]	9.60	0.05	0.92	5.20	3.40	2.07	4.07	0.19	0.10	0.52	1.37	0.32	1.93	6.42	1.53	1.08
^{3}He/^{4}He	8.20	8.06	8.78	8.30	7.94	8.54	8.23	7.97	8.18	8.41	8.42	8.49	8.34	8.53	8.03	8.64
Powder Melt[a]																
[^{4}He]	–	–	0.052	–	–	–	6.56	–	–	–	1.29	–	–	–	–	0.097
^{3}He/^{4}He	–	–	5.05	–	–	–	8.44	–	–	–	8.45	–	–	–	–	5.83
Whole-Rock Melt[a]																
[^{4}He]	11.30	0.28	–	8.50	7.63	3.03		0.07	0.06	–	–	0.35	–	6.60	5.69	–
^{3}He/^{4}He	8.76	4.41	–	8.25	8.00	7.88		n.d.	2.11	–	–	7.60	–	6.39	8.34	–
Stepped Heating[a]																
400°C																
[^{40}Ar]	23	11	19	210	22	13	50	70	388	123	56	21	14	25	43	58
^{40}Ar/^{36}Ar	296	370	327	301	319	332	327	271	304	295	320	420	320	292	310	292
800°C																
[^{40}Ar]	1220	1056	155	275	203	239	156	773	92	348	105	58	68	167	113	62
^{40}Ar/^{36}Ar	2734	307	428	608	532	1247	637	296	301	296	432	314	387	296	281	296
1200°C																
[^{40}Ar]	33	195	83	66	2.3	6.6	123	0.6	95	72	0.5	1.9	91	294	40	89
^{40}Ar/^{36}Ar	350	291	295	314	n.d.	n.d.	302	n.d.	305	313	n.d.	n.d.	314	377	314	300
Fusion																
[^{40}Ar]	141	182	31	18	3.9	n.d.	500	9.3	640	77	22	9.2	740	3.1	12	440
^{40}Ar/^{36}Ar	286	302	295	n.d.	n.d.	n.d.	300	n.d.	295	307	n.d.	n.d.	298	296	n.d.	300

[a]All concentrations of helium in units of 10^{-6} cm^{3}STP/g and concentrations of argon in units of 10^{-9} cm^3 STP/g; n.d., not determined.

ratio of the blanks was 285 ± 20. Results for all analyses are presented in Table 1.

4. Results

4.1. Carbon and Water

[12] SMT glasses are close to saturation at their depth of collection for a vapor dominated by CO_2 and H_2O, as discussed by *Macpherson et al.* [1999] and *Newman et al.* [2000, see Figure 5]. This finding mirrors that for other back-arc basin basalts [*Macpherson and Mattey*, 1994; *Shaw et al.*, 2004]. *Newman et al.* [2000] modeled variations in dissolved concentrations to infer that CO_2, but not H_2O, was significantly degassed during eruption of SMT magma. They validated this conclusion by showing that CO_2 contents of glasses were significantly lower than those of melt inclusions trapped in olivine crystals. Therefore, we work from the assumption that CO_2 has experienced degassing during transport and/or eruption while water contents are representative of primitive melt compositions.

[13] Water concentrations range from 0.40 to 2.78 wt % (Table 2). The lower values are at the upper end of the range typical of MORB [*Michael*, 1995]. As demonstrated above, the range in H_2O reflects the changing composition of SMT glasses from MORB-like in the south to more arc-like in the north due to an increasing flux of material recycled from the subducted Pacific Plate (Figure 2). Dissolved CO_2 concentrations range from 5 to 231 ppm and there is a broad, negative correlation with H_2O, as predicted from the solubilities of these two species at relatively constant pressure [*Newman et al.*, 2000].

[14] Dissolved CO_2 possesses $\delta^{13}C$ values ranging from −33.0‰ to −7.0‰ (Table 2 and a single analysis from *Mattey et al.* [1984]). This is similar to the range of values in Lau and Manus back-arc basin glasses [*Macpherson and Mattey*, 1994; *Shaw et al.*, 2004]. The highest $\delta^{13}C$ value (−7.0‰; DS84-3-1) is found in the most southerly glass but relatively elevated values are found throughout the SMT (Figure 3b). There is no relationship between the water content and $\delta^{13}C$ values of the glasses.

[15] In general, there is a good correlation between the dissolved CO_2 concentration and the amount of CO_2 recovered from vesicles (Table 2). Similarly, the $\delta^{13}C$ values of dissolved and vesicle CO_2 covary; however, there is no consistent difference in $\delta^{13}C$ values between the two phases, as would be predicted if vapor and dissolved CO_2 were in equilibrium. Similar observations have been made in basaltic glasses from a wide range of geodynamic settings and reflect the effects of degassing [see *Macpherson et al.*, 2005a, and references therein]. $\delta^{13}C$ values of vesicle CO_2 in this study range from −6.5‰ to −29.8‰. This does not match the higher $\delta^{13}C$ values of vesicle gas recovered by crushing basaltic glass from further north in the Mariana Trough [*Alt et al.*, 1993; *Sano et al.*, 1998] but does extend the range to much lower values than previously reported.

4.2. Helium

[16] The abundance of helium ([He]) recovered from vesicles varies from 0.1 to 9.6 × 10^{-6} cm^3 STP/g (Figure 3c), which falls within the range observed in the Lau and Manus back-arc basins [*Poreda and Craig*, 1989; *Poreda*, 1985; *Hilton et al.*, 1993; *Macpherson et al.*, 1998] although both these basins have lower values. In this respect, the range reported here is more similar to that of MORB [*Graham*, 2002]. $^3He/^4He$ ratios of the vesicle gas show restricted variation, with a mean value of 8.3 R_A (±0.2, n = 15; where R_A is the atmospheric ratio of 1.4 × 10^{-6}) which is indistinguishable from MORB (Figures 3d and 4) and the central spreading center of the Lau Basin [*Hilton et al.*, 1993].

[17] Dissolved helium characteristics were mostly determined by mass balance (subtracting vesicle component from whole-rock melt analysis) and so are subject to greater uncertainty than vesicle analyses. In general, however, dissolved He concentrations are lower than vesicle concentrations, with a larger range in $^3He/^4He$ (Figures 3c and 3d). A single $^3He/^4He$ ratio calculated for dissolved He plots substantially higher than the mean (11.9 R_A; DS84-3-1). However, we do not believe this value indicates the presence of a high-$^3He/^4He$ component in the Mariana mantle (compare to Manus Basin [*Macpherson et al.*, 1998]): rather, it is probably an artifact of the mass balance calculation, as reflected in the large uncertainty (Figure 3d). The remaining $^3He/^4He$ ratios of dissolved He are similar to, or lower, than MORB. In contrast to the findings of *Poreda* [1985], there is no evidence for a relationship between the concentration of water and $^3He/^4He$ in the SMT suite.

4.3. Argon

[18] Abundances of argon ([Ar]) in vesicle gas vary from 58 to 1220 × 10^{-9} cm^3 STP/g. Like He,

Table 2. H_2O, CO_2, He, and Ar Concentrations and Isotopic Ratios for Southern Mariana Trough Basaltic Glasses

	Southern SMT					Northern SMT										
	84-3-1	86-4-2	86-6	88-1-1	88-1-4	80-5-1	79-2-1	18-1-3	74-1-1	74-2-4	74-3-2	74-5-1	73-1-2	71-1-1	71-3	69-1-2
SiO_2	51.32	50.80	51.57	61.32	–	–	50.91	50.92	–	–	51.47	–	–	51.46	49.02	–
MgO	7.74	5.29	6.44	6.40	–	–	7.48	6.66	–	–	7.73	–	–	6.73	7.87	–
Mg number	67	51	58	60	–	–	67	64	–	–	68	–	–	67	67	–
K/Ti	0.135	0.385	0.209	0.255	–	–	0.337	0.457	–	–	0.299	–	–	0.451	0.364	–
							Dissolved									
H_2O[a] (ppm)	0.40	0.58[b]	0.59	–	1.35	2.78[b]	1.14	2.03[b]	–	1.93	1.15	2.07[b]	–	1.59	1.07	–
CO_2[a] (ppm)	231.0	96.5	146.1	204.5	148.1	134.4	157.5	28.1	4.6	29.0	104.7	14.3	117.4	136.8	142.5	–
$\delta^{13}C$[a] (‰)	−7.0	−10.6	−10.1	−9.0	−8.9	−7.4	−8.2	−14.5	−24.4	−33.0	−7.4	−14.5	−8.3	−7.3	−9.0	–
^4He ($\times10^{-6}$ cm^3 STP/g)	1.70[c]	0.22[c]	0.05	3.30[c]	4.20[c]	0.96[c]	6.56	–	–	–	1.29	0.03[c]	–	0.18[c]	4.16[c]	0.10
2σ	1.04	0.02	0.01	0.68	0.55	0.26	0.64				0.13	0.03		0.62	0.36	0.01
$^3He/^4He$	11.9[c]	3.6[c]	5.1	8.2[c]	8.0[c]	6.5[c]	8.4	–	–	–	8.5	–	–	–	8.5[c]	5.8
2σ	2.7	2.0	0.4	1.8	1.8	1.6	0.2				0.3				2.1	0.5
^{40}Ar ($\times10^{-9}$ cm^3 STP/g)	33	195	83	66	2.3	6.6	123	0.6	95	72	0.5	1.9	91	294	40	89
2σ	9	26	13	11			12		18	16			9	8	13	15
$^{40}Ar/^{36}Ar$	350	291	295	314	–	–	302	–	305	313	–	–	314	377	314	300
2σ	150	60	70	80		–	45	–	85	105	–	–	45	16	150	87
							Vesicle									
CO_2[a] (ppm)	297.5	76.4	149.1	120.2	120.1	192.5	100.3	30.9	6.5	–	95.0	9.1	99.3	114.2	104.0	–
$\delta^{13}C$[a] (‰)	−6.5	−11.6	−9.6	−9.5	−10.8	−9.4	−12.3	−19.4	−29.8	–	−10.2	−13.8	−8.5	−10.6	−9.2	–
^4He[d] ($\times10^{-6}$ cm^3 STP/g)	9.60	0.05	0.92	5.20	3.40	2.07	4.07	0.19	0.10	0.52	1.37	0.32	1.93	6.42	1.53	1.08
$^3He/^4He$[d]	8.2	8.1	8.8	8.3	7.9	8.5	8.2	8.0	8.2	8.4	8.4	8.5	8.3	8.5	8.0	8.6
^{40}Ar ($\times10^{-9}$ cm^3 STP/g)	1220	1056	155	275	203	239	156	773	92	348	105	58	68	167	113	62
2σ	3	5	2	2	2	2	2	3	3	3	2	3	2	1	2	10
$^{40}Ar/^{36}Ar$	2734	307	428	608	532	1247	637	296	301	296	432	314	387	296	381	296
2σ	44	4	13	14	13	45	20	3	20	5	14	32	20	5	15	22
$^4He/^{40}Ar^*$[e]	8.8	1.4	19.2	36.8	37.8	11.4	48.7	–	65.4	–	41.4	96.2	121.1	–	60.7	–
$CO_2/^3He$ ($\times10^9$)	1.39	66.01	6.88	1.03	1.64	4.02	1.10	–	2.94	–	3.04	1.24	2.28	–	3.12	–
$CO_2/^{40}Ar^*$ ($\times10^6$)	0.14	1.03	1.59	0.43	0.68	0.54	0.61	–	2.17	–	1.46	1.40	3.17	–	2.10	–

[a]CO_2 and H_2O determinations conducted on single glass splits by stepped heating extraction [*Macpherson et al.*, 1999].
[b]Water concentrations determined by FTIR [*Newman et al.*, 2000].
[c]Dissolved He concentration and $^3He/^4He$ determined by mass balance from crush and whole-rock melt experiments reported in Table 1.
[d]2σ for vesicle [He] < 5% and for vesicle $^3He/^4He$ < 3%.
[e]$^{40}Ar^* = (^{40}Ar/^{36}Ar - 296) \times ([^{40}Ar]/^{40}Ar/^{36}Ar)$.

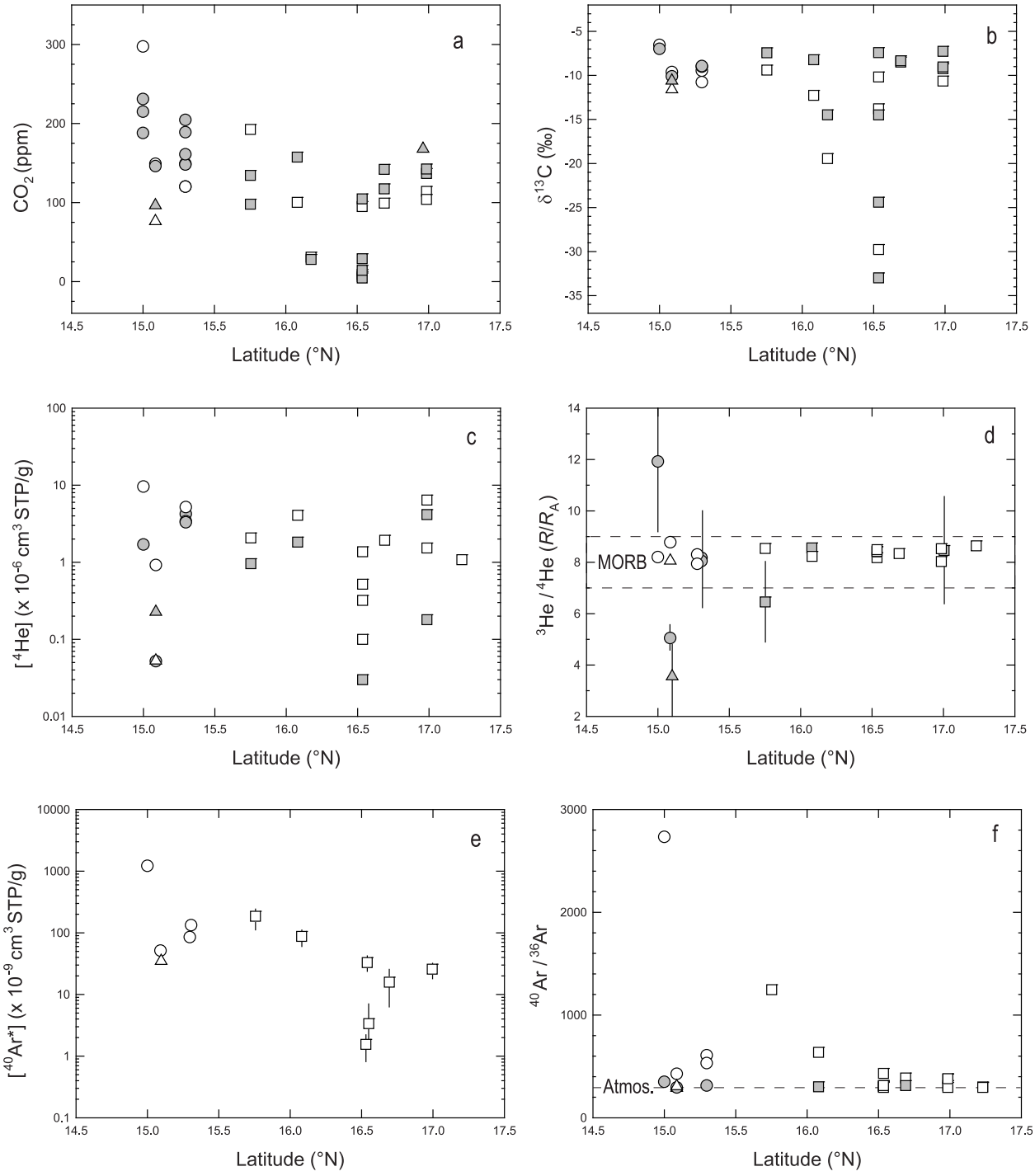

Figure 3. Latitudinal variations in (a) CO_2 content, (b) $\delta^{13}C$, (c) He content, (d) $^3He/^4He$, (e) $^{40}Ar^*$, and (f) $^{40}Ar/^{36}Ar$ of vesicle (open symbols) and dissolved (solid symbols) volatile components in Southern Mariana Trough basaltic glasses. Dashed lines in Figure 3d give the range of MORB $^3He/^4He$, while the horizontal line in Figure 3f gives the isotopic ratio of atmospheric argon.

this range is similar to that determined for Lau and Manus back-arc basin basalt [*Hilton et al.*, 1993; *Shaw et al.*, 2004]. $^{40}Ar/^{36}Ar$ varies from atmospheric values of 286 up to 2734 (Figure 3f) and encompasses most of the range previously found for the Mariana Trough, excepting one value of 5000 found at 18°N [*Ikeda et al.*, 1998; *Sano et al.*, 1998]. The range is also similar to that of the

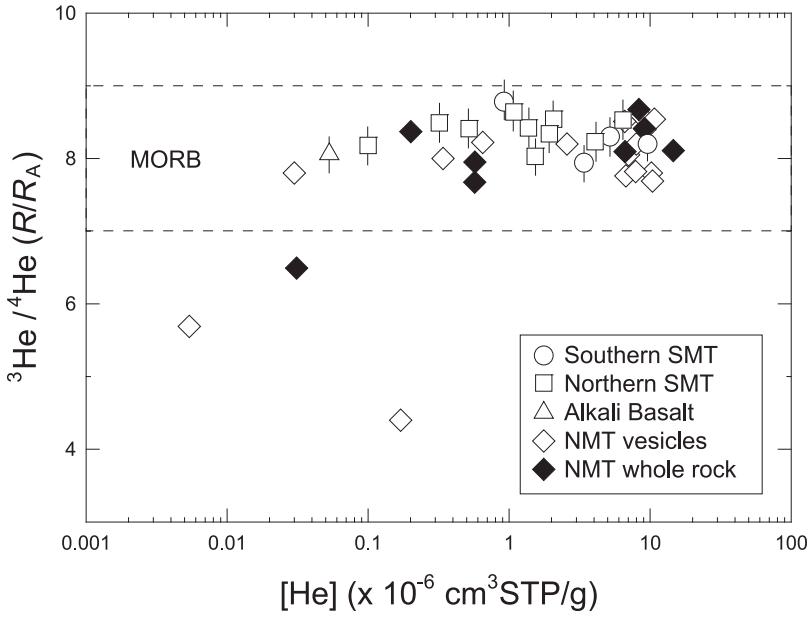

Figure 4. Plot of ^{3}He/^{4}He versus [He] for vesicle gas from the Southern Mariana Trough (SMT) basaltic glasses. Data for Northern Mariana Trough (NMT) sites are from *Poreda* [1985], *Ikeda et al.* [1998], and *Sano et al.* [1998]. *Ikeda et al.*'s [1998] data are whole-rock fusion (vesicle plus dissolved components) but show no systematic difference from other NMT data. The typical range of ^{3}He/^{4}He in MORB (8 ± 1 RA [*Graham*, 2002]) is shown by the dashed lines.

Manus Basin but does not reach the highest values found in Lau Basin basalts (5860 [*Hilton et al.*, 1993]).

[19] The highest ^{40}Ar/^{36}Ar ratio in the SMT suite was found in vesicles from the most gas-rich, H_2O-poor glass (DS84-3-1) in the south: all other S-SMT samples have vesicle ^{40}Ar/^{36}Ar ratios <610 (Figure 3f). Vesicle ^{40}Ar/^{36}Ar values in the N-SMT are generally close to atmosphere (<430) save for two localities at the southern extreme where values are 640 and 1250 (Figure 3f). In vesicle gas, values for ^{40}Ar*; the nonatmospheric portion of ^{40}Ar, decrease from south to north and correlate with ^{4}He/^{40}Ar*, an important degassing index (Figure 5). Dissolved [Ar] is variable but mostly lower than vesicle-sited gas (<300 × 10^{-9} cm^3 STP/g; Figure 3e). ^{40}Ar/^{36}Ar ratios for dissolved Ar are no higher than 380, with most being close to the atmospheric ratio (Table 2).

5. Volatile Evolution During Magma Transport and Emplacement

[20] Volatile components are hosted in magma in two principal forms: either dissolved in the melt or exsolved into a fluid/gas phase. By targeting dissolved (glass) and vesicle-sited components, it is possible to evaluate the features of each and to place constraints on both the degassing history of SMT magmatism and the nature of underlying mantle sources.

5.1. Dissolved Volatiles

[21] *Newman et al.* [2000] used the CO_2 and H_2O contents in melt inclusions of phenocrysts in SMT lavas to calculate entrapment depths of 3 to 7 km beneath the seafloor. These data demonstrate that SMT magmas contained appreciable quantities of CO_2 when the melt inclusions were trapped, while the CO_2 and H_2O saturation of SMT glasses demonstrates that much of the volatile inventory present at entrapment was lost during transport to eruption sites. Such gas loss would act to fractionate the isotopes of carbon, resulting in differences in δ^{13}C between CO_2 in the melt and vapor phases [*Pineau and Javoy*, 1983]. Therefore, carbon isotope ratios can be used to place further constraints on degassing.

5.1.1. Isotopic Evolution of Dissolved CO_2

[22] The isotopic evolution of magmatic CO_2 during degassing can be described by two end-member

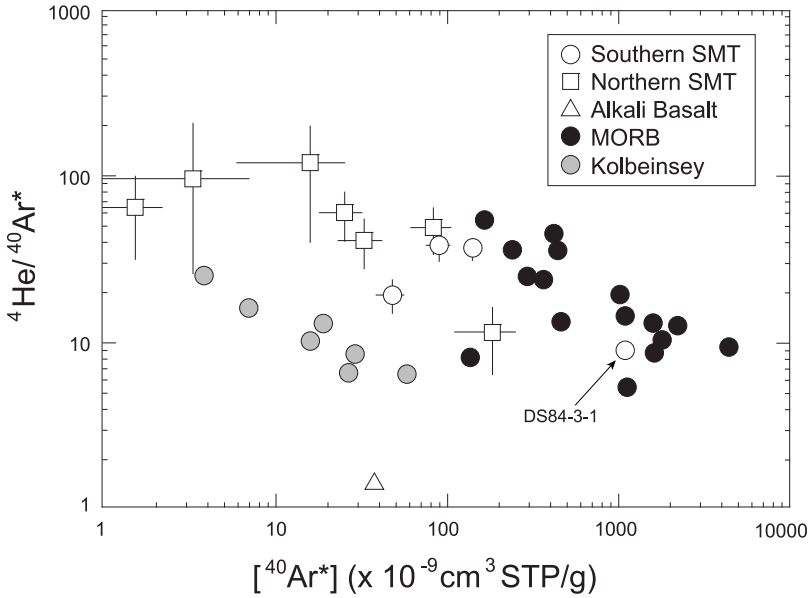

Figure 5. Plot of $^4He/^{40}Ar^*$ versus $^{40}Ar^*$ for vesicle gas from the Southern Mariana Trough (SMT) basaltic glasses. Data for Southern Kolbeinsey Ridge basaltic glasses [*Macpherson et al.*, 2005a] and normal mid-ocean ridge basalt (MORB [*Moreira and Sarda*, 2000]) are shown for comparison.

processes [*Gerlach and Taylor*, 1990]. Throughout batch equilibrium degassing (BED), or closed system degassing, vapor maintains isotopic equilibrium with the melt from which it exsolves. Fractional equilibrium degassing (FED), or open system degassing, occurs when vapor forms in isotopic equilibrium with a melt then becomes isolated from the melt phase before further exsolution occurs. The extent to which ^{13}C and ^{12}C are partitioned by degassing will depend on the fractionation factor ($\alpha_{CO2\text{-}melt}$) between CO_2 dissolved as carbonate ions in basaltic melt [*Fine and Stolper*, 1986] and free CO_2 in the vapor phase.

[23] Variations in the concentrations and $\delta^{13}C$ values of dissolved CO_2 in SMT glasses are consistent with simple equilibrium degassing of a common parental composition. Figure 6 demonstrates that most samples can be bracketed between, and cluster close to one of, two trends emanating from a restricted range of CO_2 and $\delta^{13}C$ values. There is a shallow trend with relatively high $\delta^{13}C$ values, which approximates BED, and a second, steeper trend with increasingly low $\delta^{13}C$ values at low CO_2, resembling an FED trend. The single sample from 18°N [*Mattey et al.*, 1984] also lies close to the BED trend. Two N-SMT samples, both from site 74, possess substantially lower $\delta^{13}C$ values than other samples with similar CO_2 concentrations. While it is possible that the low $\delta^{13}C$ represents posteruptive contamination on glass surfaces, every precaution was taken in cleaning these glasses prior to stepped heating analysis [*Macpherson et al.*, 1999]: therefore, we consider this an unlikely possibility. Alternatively, these two glasses were derived from magma with lower primitive $\delta^{13}C$ values than the rest of the SMT suite. However, no other geochemical feature of these samples suggests that they were derived from a source different to the rest of the N-SMT [*Gribble et al.*, 1996]. Therefore, the most likely explanation for these two data is that they were derived from similar preeruptive magma as other N-SMT melts but acquired low $\delta^{13}C$ during interaction with the crust [*Macpherson et al.*, 2005a].

[24] Dissolved CO_2 concentrations are consistent with saturation at the pressure of eruption [*Newman et al.*, 2000] so much of the CO_2 and $\delta^{13}C$ variation in the suite is likely to be the result of degassing during eruption. Convergence of $\delta^{13}C$ values at high CO_2 concentrations indicates that this variation was produced from preeruptive magmas that were very similar, perhaps identical, with respect to carbon. *Macpherson and Mattey* [1994] demonstrated that such BED and FED trends can be exploited to determine $\alpha_{CO2\text{-}melt}$ and preeruptive CO_2 concentrations and $\delta^{13}C$ values. First, the slope of best fit to the FED trend in Figure 6 yields $\alpha_{CO2\text{-}melt}$. The value of $\alpha_{CO2\text{-}melt}$ derived for SMT samples is 2.3‰ ($R^2 = 0.94$), in excellent agreement with values determined for equilibrium

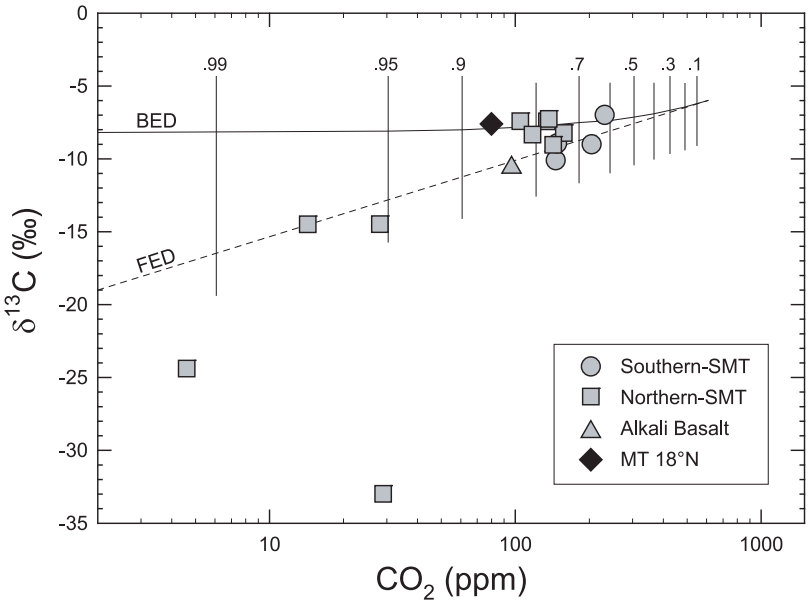

Figure 6. Plot of $\delta^{13}C$ versus concentration of CO_2 dissolved in Southern Mariana Trough (SMT) basaltic glasses. A single analysis of dissolved CO_2 from a Northern Mariana Trough glass (black diamond [*Mattey et al.*, 1984]) is shown for comparison. Curves illustrate batch equilibrium degassing (BED; solid curve) and fractional equilibrium degassing (FED; dashed curve) models for a preeruptive melt with composition calculated from SMT data using the method of *Macpherson and Mattey* [1994] and $\alpha_{CO2\text{-}melt}$ of 2.3‰. Vertical lines indicate the fraction of CO_2 lost along each curve.

between gaseous CO_2 and calcite at magmatic temperatures [*Scheele and Hoefs*, 1992] and for a number of prior studies of basalt glasses (as discussed in detail by *Macpherson et al.* [2005a]). The approach of *Macpherson and Mattey* [1994] generates a single estimate of the preeruptive melt composition (C_p) and two separate estimates of preeruptive $\delta^{13}C$ (δ_p). Using the SMT data reported here, we obtain 605 ppm for C_p, and δ_p values of −5.5‰ and −6.1‰. Degassing of this composition (with the mean δ_p value) is illustrated in Figure 6 and suggests that the least degassed Mariana Trough glasses were quenched upon eruption onto the seafloor having lost approximately 60% of their preeruptive CO_2 while the most degassed samples have lost >95% of this preeruptive amount.

5.1.2. Implications of Dissolved CO_2 Variations

[25] The degassing model described above highlights four striking features of the SMT data set. First, given that the average depth of collection of *Sonne* 69 samples is 3.8 km beneath sea level [*Gribble et al.*, 1996] then the C_p value calculated from dissolved CO_2 concentrations would imply saturation at ~3.3 km beneath the ridge axis. *Kitada et al.* [2006] used gravity anomalies to estimate crustal thickness of 4 to 5.5 km for the SMT. Thus, the preeruptive dissolved CO_2 concentration suggests melt reached vapor saturation in the deeper parts of the crust. Saturation at such depths is consistent with volatile concentrations in olivine-hosted melt inclusions [*Newman et al.*, 2000]. However, *Newman et al.* [2000] also found melt inclusions in plagioclase containing higher CO_2 concentrations that equate to entrapment at 6 to 7 km beneath the ridge axis. Therefore, we infer that phenocrysts were forming and melt degassing was active in the deep crust or shallow mantle beneath the SMT spreading system.

[26] Second, only two samples (from site 74) do not conform to the degassing model (Figure 6). As noted above, these very low $\delta^{13}C$ values could result from assimilation of shallow crust, as observed for the southern Kolbeinsey Ridge, adjacent to Iceland [*Macpherson et al.*, 2005a]. The lack of more samples with very low $\delta^{13}C$ may indicate most magma escaped interaction with crust. Alternatively, wall rock may have had magma-like $\delta^{13}C$ values and so caused negligible modification to the isotopic composition of the magma. In this respect, Mariana samples resemble the Central Lau back-arc basin, where $\delta^{13}C$ values of dissolved CO_2 are controlled primarily by degassing yet $\delta^{18}O$ data demonstrate that many melts interacted

with hydrothermally altered crust [*Macpherson and Mattey*, 1994, 1998]. The distinctive carbon isotopic signature of magma-crust interaction at Kolbeinsey may relate to its much thicker crust and, hence, lower geothermal gradient. Both properties could contribute to greater $\delta^{13}C$ diversity between the seafloor and the 3–4 km depth where magma ponded.

[27] Third, there is no distinction in the carbon systematics of S-SMT and N-SMT glasses. The northern and southern segments of the SMT have different crustal thickness [*Kitada et al.*, 2006] and fluxes of recycled components (Figure 2), therefore, differences in CO_2 degassing style and/or source composition might be anticipated. For example, back-arc magmatism in the Lau Basin demonstrates that different degassing regimes are associated with propagating versus dying ridge segments [*Macpherson and Mattey*, 1994]. Yet BED and FED behavior is displayed by samples from both the N-SMT and S-SMT (Figure 6). Despite the strong evidence from H_2O and lithophile elements for distinct sources for S-SMT and N-SMT magmatism, this difference is not manifested in carbon isotopic ratios.

[28] Finally, the carbon isotopic composition of preeruptive SMT magma lies within the $\delta^{13}C$ range of the upper mantle [*Deines*, 2002] and is similar to preeruptive $\delta^{13}C$ values for magma from other back-arc basins and from mid-ocean spreading centers, both proximal and distal to hot spots [*Macpherson and Mattey*, 1994; *Pineau and Javoy*, 1994; *Cartigny et al.*, 2001; *Macpherson et al.*, 2005a]. The preeruptive $\delta^{13}C$ value may not be representative of primary SMT magma since CO_2 degassing is likely to have occurred prior to, or during, storage near the base of the crust (section 5.2). The assumed preeruptive CO_2 content of 605 ppm is less than the highest concentration (875 ppm) measured in any melt inclusions from the Mariana Trough [*Newman et al.*, 2000]. If 875 ppm represents the CO_2 concentration in parental magma then the calculated preeruptive melt must have lost ~30% of its initial CO_2. This would have lowered the $\delta^{13}C$ value by ~0.70‰ ($\alpha_{CO2\text{-}melt}$ of 2.3‰ and assuming that preeruptive degassing occurs through BED [*Pineau and Javoy*, 1983]). Notably, initial CO_2 concentration estimates from the melt inclusions are minima. Any higher initial content would infer correspondingly higher $\delta^{13}C$, up to a maximum value equal to the preeruptive $\delta^{13}C$ plus $\alpha_{CO2\text{-}melt}$, i.e., −3.4‰. It is not possible to place further constraints on the characteristics of initial CO_2 from the dissolved component alone, but we shall return to this issue during discussion of the vapor phase.

5.1.3. Summary of Dissolved Components

[29] Helium and argon data for the dissolved phase are consistent with the model developed from the major volatiles. With the exception of sample DS84-3-1 (see above), glasses containing the highest concentrations of dissolved He possess $^3He/^4He$ ratios that are indistinguishable from MORB (Table 2). $^3He/^4He$ ratios that lie significantly below the mean value for vesicles occur in He-poor samples (Table 2). A similar relationship is observed in lavas from a range of geodynamic environments and, since exsolution of a gas phase should not fractionate the isotopes of helium, is attributed to contamination of low-[He] magma by existing crust, which can be ^4He-rich [*Hilton et al.*, 1993, 1995; *van Soest et al.*, 2002; *Day et al.*, 2005; *Macpherson et al.*, 2005a, 2005b]. Like carbon, $^3He/^4He$ values of the least degassed samples suggest that there is no isotopic distinction between the sources of S-SMT and N-SMT glasses. Dissolved $^{40}Ar^*$ values are lower than 10×10^{-9} cm^3 STP/g, suggesting substantial degassing of Ar. $^{40}Ar/^{36}Ar$ ratios are very low, close to atmospheric ratios (Figure 5).

[30] In summary, CO_2, He and Ar data reveal evidence for variable, and in some case extensive, degassing. Two features suggest that some SMT magma experienced open system degassing during eruption. First, several glasses show combined dissolved CO_2-$\delta^{13}C$ systematics that are consistent with open system degassing (FED; Figure 6). Second, few of the SMT glasses show carbon isotopic equilibrium between the dissolved and gas phases. The apparent influence of interaction with wall rock components during transport is stronger for $^3He/^4He$ than $\delta^{13}C$. As noted above, the thin Mariana crust may have resulted in degassing and magma storage occurring at, or even beneath, the base of the crust at levels where there is little carbon isotopic contrast between magma and contaminant.

5.2. Vesicle Gases

[31] Intervolatile ratios and isotopic ratios of vesicle gas provide a valuable record of the integrated degassing history of magmatic vapor. In this section, we use these relationships to place constraints on the preeruptive degassing mechanisms and volatile composition of parental SMT magma. Intervolatile ratios of vapor depend on the solubility of each volatile species in the melt phase. Solubility is a function of melt structure and so can change with composition but these changes are minor in the restricted range of basaltic compositions [*Carroll and*

Webster, 1994; *Dixon and Stolper*, 1995]. Therefore, changes in basalt chemistry, alone, produce negligible fractionation between volatiles, although variations in the amount of water dissolved in melt can profoundly influence the solubility of other volatile species [*Dixon and Stolper*, 1995; *Paonita et al.*, 2000]. For any particular batch of magma there are then two further properties that affect solubility and, hence, the fractionation of different volatile species; pressure and melt volume.

[32] Pressure exerts the strongest control on solubility variations in any single batch of magma. Solubilities are reduced as the confining pressure on the melt decreases resulting in exsolution of volatiles into a free vapor/fluid phase. There will be differential partitioning of volatiles between the melt and vapor with respect to one another due to their different solubilities. This is the primary cause of volatile fractionation as magma decompresses when it is transported toward the surface.

[33] Volatile species are incompatible in most crystalline phases and so, as magma crystallizes, the concentration of each volatile dissolved in the melt will increase until it reaches saturation. Once saturated, the dissolved concentration of a volatile will be buffered by its solubility and any excess will exsolve into the vapor phase as crystallization decreases the volume of melt. Therefore, crystallization can also drive degassing and, hence, intervolatile fractionation [*Marty and Zimmermann*, 1999; *Marty et al.*, 2001; *Macpherson et al.*, 2005a]. This phenomenon will be enhanced in hydrous magma because H_2O, due to its high solubility, will continue to behave as an incompatible component after CO_2 and noble gases are saturated. Progressive crystallization will, therefore, increase the concentration of H_2O and, thus, further decrease the solubility of CO_2 (see above). Crystallization can also provide a source of heat to mobilize volatile components stored in the crust or shallow mantle, resulting in assimilation with degassing.

[34] The interplay of solubility, pressure change and crystallization has the potential to produce a diverse range of properties in the volatile components of any one batch of magma. Volatile fractionation operating during transport through, or storage within, the mantle and crust will then be overprinted by the effects of eruptive degassing. Therefore, to understand the SMT vesicle gases we first identify the variations in intervolatile ratios of vesicle gas generated during eruption. Such an approach requires identification of the sample(s) likely to have experience the least degassing. This can be achieved using noble gas ratios [*Burnard*, 2001; *Burnard et al.*, 2004]. He is more soluble in basaltic magma than Ar, therefore $^4He/^{40}Ar^*$ should increase in the residue as degassing proceeds. The maximum $^4He/^{40}Ar^*$ that can be generated during closed system degassing is the product of the solubility ratio ($S_{He}/S_{Ar} \sim 9.5$ [*Jambon et al.*, 1986]) and the initial $^4He/^{40}Ar$ value*. Estimates of $^4He/^{40}Ar^*$ in the upper mantle lie in the range 2–3 [*Marty and Zimmermann*, 1999; *Burnard*, 2001] so vesicle $^4He/^{40}Ar^*$ ratios in excess of ~35 in several SMT glasses (Table 2) confirm the conclusion, based on dissolved volatiles (section 5.1), that open system behavior occurred during at least some of the degassing history.

[35] Only one SMT glass possesses $^4He/^{40}Ar^*$ close to the range of estimated upper mantle values (Figure 5). This is the alkali basalt (DS86-4-2) but it also displays highly distinctive $CO_2/^3He$ and $CO_2/^{40}Ar^*$ (Figure 7). This difference, in conjunction with discrepancies in whole-rock geochemistry, suggests that the alkali basalt was derived from a distinct source and/or melting regime to the more silica-saturated magmas [*Gribble et al.*, 1996]. DS84-3-1 displays the lowest $^4He/^{40}Ar^*$ (8.8) among the tholeiitic glasses. To achieve this $^4He/^{40}Ar^*$ value from an initial melt value resembling upper mantle (2 or 3) would require ~60% to 70% closed system degassing, which is consistent with the conclusions reached for dissolved carbon (section 5.1.2). The increasing $^4He/^{40}Ar^*$ with decreasing $^{40}Ar^*$ of vesicle gas in the whole SMT suite is similar to that seen in other suites of glasses where degassing is thought to exert a major control on volatile fractionation (Figure 5). Therefore, we treat the vesicle gas in DS84-3-1 as representing the least degassed SMT vapor after transfer from the mantle source to storage near the base of the crust. This provides our starting point for models of eruptive degassing.

5.2.1. Eruptive Degassing

[36] To explore the intervolatile fractionation that might be generated by eruptive degassing from the composition of DS84-3-1, we first determined BED and FED models using relative solubilities of $S_{He}/S_{CO2} = 2.4$ [*Hilton et al.*, 1998] and $S_{CO2}/S_{Ar} = 4$ [*Cartigny et al.*, 2001]. This should lead to increases in $^4He/^{40}Ar^*$ and $CO_2/^{40}Ar^*$, and decreases in $CO_2/^3He$. Figures 7a–7c show that BED (short dashed lines) and FED (solid lines) do not reproduce the variation of the whole SMT suite. FED of a subset of samples, the low-$CO_2/^3He$ group ($CO_2/^3He$: 1.03 to 1.64 × 10^9), is consistent with variations of $^4He/^{40}Ar^*$ versus $CO_2/^3He$ and $CO_2/^{40}Ar^*$

versus $CO_2/^3He$ (Figures 7a and 7b). However, the FED model displays a poor fit for $^4He/^{40}Ar^*$ versus $CO_2/^{40}Ar^*$, with a steeper slope than the low-$CO_2/^3He$ array (Figure 7c). This discrepancy can be resolved by doubling the solubility of CO_2 with respect to He and Ar, such that $S_{He}/S_{CO2} = 1.2$ and $S_{CO2}/S_{Ar} = 8$. Due to different dissolution mechanisms, enhanced CO_2 solubility with respect to noble gases is predicted for basaltic magmas at higher pressures [*Burnard*, 2001]. This modification has

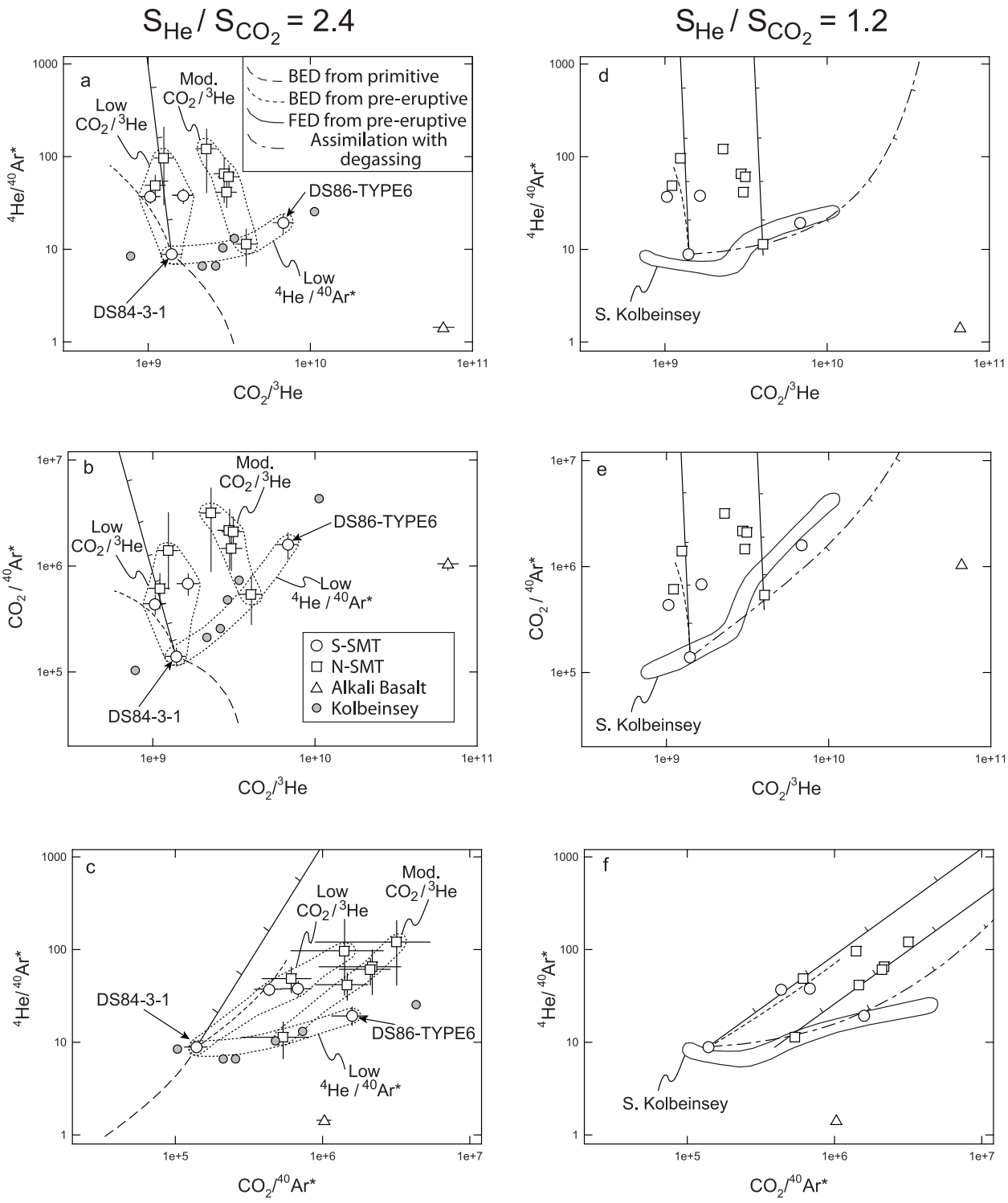

Figure 7

no detrimental effect upon the quality of fit to the data for $^4He/^{40}Ar^*$ versus $CO_2/^3He$ and $CO_2/^{40}Ar^*$ versus $CO_2/^3He$ (Figures 7d and 7e) but does produce a better fit for $^4He/^{40}Ar^*$ versus $CO_2/^{40}Ar^*$ (Figure 7f). The difference between the eruptive FED and BED models is also significantly reduced by modifying the relative solubilities, although BED is unable to produce the full range of intervolatile ratios, notably the elevated $^4He/^{40}Ar^*$, displayed by the low-$CO_2/^3He$ group. Therefore, simple BED and FED models can reproduce the variation observed in vesicle gases of those samples with relatively low $CO_2/^3He$.

[37] With the exception of DS86-TYPE6, the remaining tholeiites form an array that is subparallel to the low-$CO_2/^3He$ group but displaced to higher CO_2. Therefore, this moderate-$CO_2/^3He$ group ($CO_2/^3He$: 2.28 to 4.02 × 10^9) is also consistent with degassing but starting from more elevated $CO_2/^3He$ and $CO_2/^{40}Ar^*$. Figures 7d–7f illustrate that FED for a starting composition containing three times the CO_2 of DS84-3-1, such that $CO_2/^3He = 4 \times 10^9$ and $CO_2/^{40}Ar^* = 400{,}000$, corresponds well to the moderate-$CO_2/^3He$ group. BED models (not shown in Figures 7d–7f) would be compatible with some of the variation but cannot produce the entire range of intervolatile ratios displayed by these samples.

[38] Thus, the majority of $^4He/^{40}Ar^*$ variation in vesicle gases can be explained by degassing that occurred during eruption, but not from a unique starting composition. The low-$CO_2/^3He$ group represents eruptive degassing of vapor from a starting point that resembled DS84-3-1, while the moderate-$CO_2/^3He$ group could have resulted from eruptive degassing from an initial composition containing approximately three times as much carbon as DS84-3-1. DS86-TYPE6 indicates existence of vapor with even higher $CO_2/^3He$. In $^4He/^{40}Ar^*$-$CO_2/^3He$-$CO_2/^{40}Ar$ space this sample plots on an extension from DS84-3-1 through the lowest $^4He/^{40}Ar^*$ member of the moderate-$CO_2/^3He$ group (Figure 7). $CO_2/^3He$ and $CO_2/^{40}Ar^*$ ratios of DS86-TYPE6 indicate carbon enrichment of approximately five times, relative to DS84-3-1. Therefore, we infer the existence of a high-$CO_2/^3He$ group. The least degassed members of the three groups cannot be related to one another by eruptive degassing and probably represent a spectrum of different $CO_2/^3He$ (and $^4He/^{40}Ar^*$ and $CO_2/^{40}Ar^*$) values that were present when magma was stored beneath the ridge, upon which the effects of eruptive degassing were superimposed. For simplicity, we will continue to refer to the three discrete groups. However, determining the origin of their least degassed (i.e., lowest $^4He/^{40}Ar^*$) members, which henceforth we shall refer to as the low-$^4He/^{40}Ar^*$ array (Figure 7), is the next step in understanding the volatile history of SMT magmatism.

5.2.2. Carbon Enrichment During Preeruptive Storage

[39] Variations in $CO_2/^3He$ have been used in several subduction systems to infer recycling of subducted carbon [*Hilton et al.*, 2002, and references therein]. However, two observations lead us to question whether such an explanation is applicable for the SMT glasses. First, the CO_2 enrichments are not consistent with the south to north increase in apparent recycled fluxes displayed by other geochemical tracers in SMT glasses [*Gribble et al.*, 1996]. Instead, some N-SMT glasses lie among the low-$CO_2/^3He$ group, while the highest $CO_2/^3He$ tholeiite (DS86-TYPE6) is from the S-SMT. Experimental petrology and numerical simulations both predict that carbon and water can be decoupled during slab devolatilization but both approaches indicate preferential retention of carbon in the slab at depths coincident with the back arc [*Kerrick and Connelly*,

Figure 7. Plots of (a) $^4He/^{40}Ar^*$ versus $CO_2/^3He$, (b) $CO_2/^{40}Ar^*$ versus $CO_2/^3He$, and (c) $^4He/^{40}Ar^*$ versus $CO_2/^{40}Ar^*$ in vesicle gas from Southern Mariana Trough (SMT) basaltic glasses. Data for Southern Kolbeinsey Ridge basaltic glasses are shown for comparison [*Macpherson et al.*, 2005a]. Dotted lines enclose various groups discussed in the text. Batch equilibrium degassing (BED) models were calculated using the method of *Jambon et al.* [1986]. BED models are shown for the effects of degassing prior to and after preeruptive storage and show degassing from zero (low $^4He/^{40}Ar^*$) to maximum (high $^4He/^{40}Ar^*$) vesicularity. Models for eruptive fractional equilibrium degassing (Rayleigh distillation) were calculated for the ratio of two elements i and j with solubilities Si and Sj, respectively; $(i/j) = (i/j)_{initial} \times F^{[1-(Si/Sj)]}$. Tick marks on FED curves represent gas loss intervals of 10%. All models in Figures 7a–7c employ $S_{He}/S_{CO2} = 2.4$ [*Hilton et al.*, 1998] and S_{CO2}/S_{Ar} of 4 [*Cartigny et al.*, 2001]. The preeruptive melt has the same composition as sample DS84-3-1. (d–f) The same data as in Figures 7a–7c, this time with the Kolbeinsey data represented by a field. BED and FED models for eruptive degassing of DS84-3-1 are shown again, but this time they have $S_{He}/S_{CO2} = 1.2$ and S_{CO2}/S_{Ar} of 8. An FED model is also show for an initial composition with the same $^4He/^{40}Ar^*$ as DS84-3-1 but with $CO_2/^3He$ of 4.0 × 10^9 and $CO_2/^{40}Ar^*$ of 400,000. The long- and short-dashed line shows assimilation of CO_2 during fractional degassing with tick intervals at 10% gas loss intervals. See text for details.

2001; *Dasgupta et al.*, 2004; *Gorman et al.*, 2006]. Therefore, there is no basis upon which to predict a significant recycled carbon flux into the relatively water-poor sources of the S-SMT. Second, the low-$^4He/^{40}Ar^*$ array closely parallels that of Southern Kolbeinsey Ridge glasses (Figure 7), which *Macpherson et al.* [2005a] interpreted as reflecting addition of carbon to basaltic magma during storage and/or eruption at the ridge. Therefore, before giving further consideration to recycling of subducted carbon, we explore the possibility that the low-$^4He/^{40}Ar^*$ array might reflect processes operating during melt transfer and storage beneath the Mariana Trough spreading system.

[40] An important constraint in this part of the discussion comes from the isotopic composition of dissolved CO_2. If carbon that possesses distinctive $^{13}C/^{12}C$ is added to magma then its presence will be apparent in the $\delta^{13}C$ values of both the vesicle and dissolved components because isotopes will continue to exchange between the two phases [*Macpherson et al.*, 2005a]. However, as noted above, very few SMT glasses display evidence for isotopic modification of the dissolved component, beyond that resulting from degassing. This indicates that there was a negligible isotopic contrast between the magma and any added carbon. There are two possible mechanisms by which carbon with magmatic $\delta^{13}C$ values could be added to magma stored near the base of the crust; gas enrichment from deeper degassing or contamination by mantle or magmatic wall rock.

5.2.2.1. Enrichment by Fluxing of CO_2 From Deeper Magma

[41] Direct evidence for deep degassing of SMT basalt comes, first, from the difference between dissolved CO_2 concentrations in melt inclusions and in dissolved glass (section 5.1) and, second, from the elevated $^4He/^{40}Ar^*$ ratio of DS84-3-1 vesicle gas relative to upper mantle (section 5.2.1). Once generated this early stage vapor phase can migrate upward, with respect to magma, and may have infiltrated magma that has ponded at shallower levels. CO_2 fluxing of this sort was invoked in studies of a number of recent volcanic eruptions [*Spilliaert et al.*, 2006; *Aiuppa et al.*, 2007; *Barsanti et al.*, 2009; *Collins et al.*, 2009; *Blundy et al.*, 2010].

[42] Vapor exsolved at deep levels, early in the history of any melt batch, will contain not just CO_2 but noble gases also (as well as trace amounts of other volatile components). The relative abundances of these volatiles will reflect the early stage at which this vapor formed, with lower $^4He/^{40}Ar^*$, lower $CO_2/^{40}Ar^*$ and higher $CO_2/^3He$ than the initial melt [*Jambon et al.*, 1986]; that is, the ratios of this vapor would be complementary to the residue. Thus, although the absolute quantity of gaseous CO_2 in stalled magma might increase as a result of fluxing by deeper magma, this should be accompanied by decreases in the $CO_2/^{40}Ar^*$ and $^4He/^{40}Ar^*$ ratios. This is not the case for SMT (Figures 7a and 7c). Therefore, we conclude the low-$^4He/^{40}Ar^*$ array was not the result of adding gas exsolved at deep levels into low-$CO_2/^3He$, preeruptive magma.

5.2.2.2. Assimilation of Wall Rock With Fractional Degassing During Magma Storage

[43] As noted above, there is a close correspondence between the low-$^4He/^{40}Ar^*$ array and glasses from the South Kolbeinsey Ridge (Figure 7). This suggests that, like Kolbeinsey, intervolatile fractionation at the SMT may result from addition of wall rock CO_2 to magma. In contrast to Kolbeinsey, however, the extraneous CO_2 in the SMT does not have distinctive, low $\delta^{13}C$ values.

[44] The increase in $CO_2/^3He$ (and $CO_2/^{40}Ar^*$) from the least degassed members of the low-, to moderate-, to high-$CO_2/^3He$ groups is accompanied by an increase in $^4He/^{40}Ar^*$ (Figures 7d–7f). This would not be expected if the process were simply the result of adding carbon, in which case $^4He/^{40}Ar^*$ should not be affected. *Macpherson et al.* [2005a] proposed that positive correlations between $^4He/^{40}Ar^*$, $CO_2/^{40}Ar^*$ and $CO_2/^3He$ at the Southern Kolbeinsey Ridge resulted from addition of crustal carbon to magma during degassing. At Kolbeinsey, this degassing occurred during eruption. In contrast, the SMT enrichment must have developed at an earlier stage because the effects of eruptive degassing are superimposed upon the $CO_2/^3He$ increase (Figure 7). This implies that any carbon addition occurred prior to eruption but after magma had developed to the composition of DS84-3-1, i.e., during residence of magma within the crust-mantle transition region.

[45] We employ a simple coupled assimilation-fractional degassing model to determine whether this mechanism could replicate the trend through the low-$^4He/^{40}Ar^*$ array (Figures 7d–7f). DS84-3-1 contains the lowest $^4He/^{40}Ar^*$ ratio and so, again, provides the starting composition. Degassing was modeled in 1% increments using the solubilities determined from modeling eruptive degassing (section 5.2.1). After each increment the contaminant was added then the next degassing

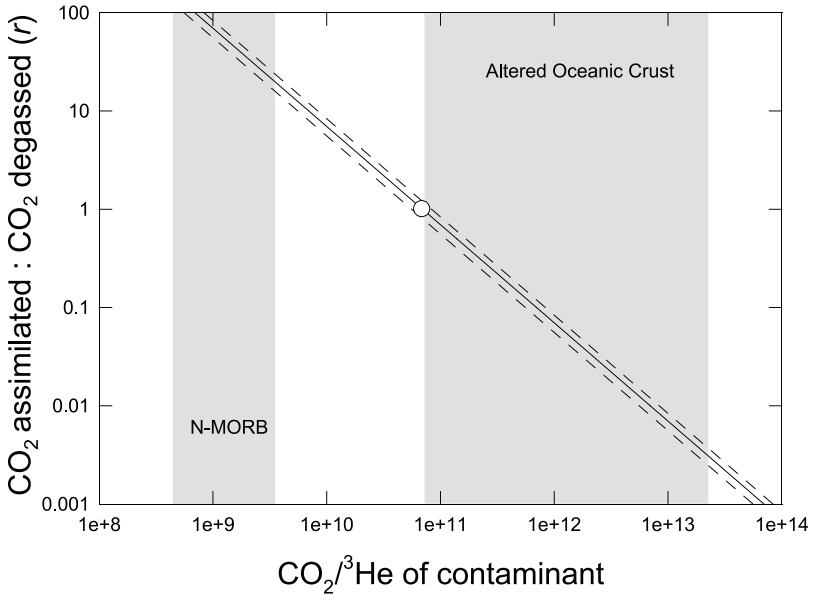

Figure 8. $CO_2/^3He$ of contaminant and ratio of assimilated to degassed CO_2 (r) in coupled assimilation-fractional degassing model. The dashed curves enclose the range of values that produce reasonable fits to the Southern Mariana Trough data, and the solid curve shows the median value of r for any given $CO_2/^3He$. The white circle represents the model illustrated in Figures 7d–7f. Shaded gray areas represent the ranges estimated for $CO_2/^3He$ in the source of NMORB [*Marty and Zimmermann*, 1999; *Resing et al.*, 2004] and in altered oceanic crust [*Hilton et al.*, 2002; *Shaw et al.*, 2004].

step calculated. The enrichment of CO_2 in the contaminant and the ratio CO_2 assimilated: CO_2 degassed (r) was varied in an attempt to find solutions that fit the low-$^4He/^{40}Ar^*$ array. The extent of degassing driven by crystallization is constrained by $^4He/^{40}Ar^*$ in DS86-TYPE6 and is limited to less than 10% (Figures 7d and 7f). Noble gases have partition coefficients in mantle phases of ≤0.01 [*Heber et al.*, 2007]; therefore, gas loss experienced at this stage will reflect the reduction in melt volume and, thus, the extent of crystallization. SMT glasses display small variations in major element concentrations and Mg numbers that are consistent with modest amounts of crystallization, around 10%, near the base of the crust [*Gribble et al.*, 1996].

[46] There is no unique model that fits the low-$^4He/^{40}Ar^*$ array. Instead a family of solutions exists in which the variation in $CO_2/^3He$ of the contaminant is inversely related to r (Figure 8). The low-$^4He/^{40}Ar^*$ array can be achieved through assimilation of material with MORB-like $CO_2/^3He$. This is also the range of $CO_2/^3He$ values that might be expected of primitive SMT basaltic rock that crystallized in the shallow mantle or deepest crust and retained a large fraction of primary volatiles, possibly in melt and/or fluid inclusions within crystals [*Kelley and Früh-Green*, 2001]. However, assimilation of material with $CO_2/^3He$ in the range 1×10^8 to 4×10^8 requires r values significantly greater than 10 (Figure 8). We view this as unlikely because, with degassing of ~10%, this would require the unlikely scenario that crystallizing melt could extract 1 to 10 times its intrinsic content of CO_2 from refractory crystalline phases.

[47] Mature oceanic crust is estimated to have extremely high $CO_2/^3He$ and so could generate the variation seen in SMT glasses with very low values of r (Figure 8). A significant portion of the carbon in mature oceanic crust is acquired through mineralization of marine CO_2 at significant distances from the ridge and is concentrated in the shallowest parts of the crust [e.g., *Alt and Teagle*, 1999]. Therefore, young, deep crust might be anticipated to contain less carbon and a $CO_2/^3He$ ratio intermediate between mantle and mature oceanic crust. However, the $CO_2/^3He$ ratio of the contaminant will depend on the nature of alteration. The noble gases are likely to have low partition coefficients for any secondary phases in the deep crust and shallow mantle. The high $CO_2/^3He$ of mature crust is due to the presence of carbonate, and young crust will also have elevated $CO_2/^3He$ if carbonate is present [*Shaw et al.*, 2004].

[48] Oceanic peridotites, both in situ and in ophiolites, can contain relatively abundant carbonate minerals

but much of this appears to be of low-temperature, nonmagmatic origin and, in some cases, is much younger than accretion of the peridotite sequence [*Bonatti et al.*, 1974; *Clark and Fontes*, 1990; *Kelemen and Matter*, 2008]. Recent observations of carbonate-bearing "diopsidite" in Oman suggest that carbonate may be stable at relatively high temperatures in altered ultramafic rocks [*Python et al.*, 2007]. While the high-temperature origin of this lithology is disputed [*Bach and Klein*, 2009], hydrothermally altered and serpentinized rocks in the shallow mantle may provide a temporary repository for CO_2 at these levels. An alternative possibility is that the shallow mantle may contain carbonate formed through the action of degassed magmatic CO_2. Several lines of evidence presented above suggest that SMT magma degassed substantial quantities of CO_2 during transportation through the shallow mantle. Reaction between supercritical CO_2 fluid and shallow mantle could produce zones of carbonate enrichment, particularly around cooling magma bodies or along established melt and/or vapor pathways. In general, carbonate is not thought to be stable in peridotite at pressures below 2 GPa [*Luth*, 1999, and references therein], but low temperatures may allow dolomite to stabilize at lower pressure [*Wyllie*, 1977; *Dalton and Wood*, 1993]. Refrigeration of shallow mantle through the action of deep-penetrating hydrothermal systems may provide an environment near active ridges in which degassed magmatic CO_2 could be incorporated as carbonate. Subsequent magma batches may then remobilize the sequestered CO_2 into the vapor phase.

[49] The carbon inventory of deep crust and shallow mantle in oceanic lithosphere is poorly constrained but the discussion above suggests that magmatic degassing and interaction with deeply penetrating hydrothermal systems may generate ephemeral carbonate reservoirs close to the crust-mantle transition. Carbonated zones produced in this way would provide a source of carbon to elevate the $CO_2/^{40}Ar^*$ and $CO_2/^3He$ values of vapor in intruding magma without causing significant modification of $\delta^{13}C$ values of either dissolved or gaseous CO_2.

5.3. Three-Stage Degassing and Storage of Degassed CO_2 at a Slow Spreading Ridge

[50] In synthesizing the degassing history of SMT magmatism there are two principal constraints that must be met: (1) Vesicle CO_2-He-Ar systematics indicate that there were at least three stages of degassing, the second of which involved addition of CO_2 to the vapor phase, and (2) $\delta^{13}C$ of dissolved CO_2 requires that assimilated carbon had a negligible influence upon the isotopic composition of the melt phase. Combining data for the dissolved and vesicle components allows us to propose the following three-stage model for evolution of SMT volatiles (Figure 9):

[51] Stage 1 is deep degassing: Melt from the mantle wedge arrives in the shallow mantle containing variable quantities of water but is sufficiently rich in volatiles to start degassing CO_2 due to decompression. This degassing lowers $\delta^{13}C$ and raises $^4He/^{40}Ar^*$ by modest amounts with respect to upper mantle starting values. Some of the CO_2 released by this degassing is incorporated in carbonated zones in the deep crust or shallow mantle. This carbonation may be assisted by the thermal and/or chemical influence of hydrothermal circulation.

[52] Stage 2 is preeruptive degassing: Magma which has stalled near the base of the crust begins to crystallize. The reduction in volume of vapor-saturated melt is small (less than ≤10%) but causes further degassing. CO_2 that was stored in wall rocks is liberated due to direct contact with magma or the action of heat released during crystallization. This CO_2 is then incorporated into magma elevating the relative carbon content of the vapor phase by up to a factor of five. The magmatic provenance of this added CO_2 means that there is no significant effect upon $\delta^{13}C$ of the melt, which will be lowered only slightly due to partitioning between melt and vapor.

[53] Stage 3 is eruptive degassing: Degassing of magma as it travels from the preeruptive storage zone to the seafloor decreases the concentration and $\delta^{13}C$ value of dissolved CO_2 and significantly increases $^4He/^{40}Ar^*$ and $CO_2/^{40}Ar^*$. This degassing had a less pronounced impact upon $CO_2/^3He$ due to the small contrast in the solubility of these two species. Interaction with shallower portions of the crust during eruption may contribute to very low $\delta^{13}C$ values in a minority of magma batches and to low $^3He/^4He$ and $^{40}Ar/^{36}Ar$ in magma that retains very little magmatic noble gas.

[54] The effects of eruptive degassing are recognized in magmatic suites from a wide variety of locations and significant headway has been made in understanding the degassing processes that operate during eruption [*Pineau and Javoy*, 1983, 1994; *Hilton et al.*, 1993, 1995, 1998; *Macpherson and Mattey*, 1994; *Dixon and Stolper*, 1995; *Burnard et al.*, 1997, 2004; *Marty and Zimmermann*, 1999; *Newman et al.*, 2000; *Burnard*, 2001; *Cartigny et al.*, 2001]. This study contributes to a growing body of evidence

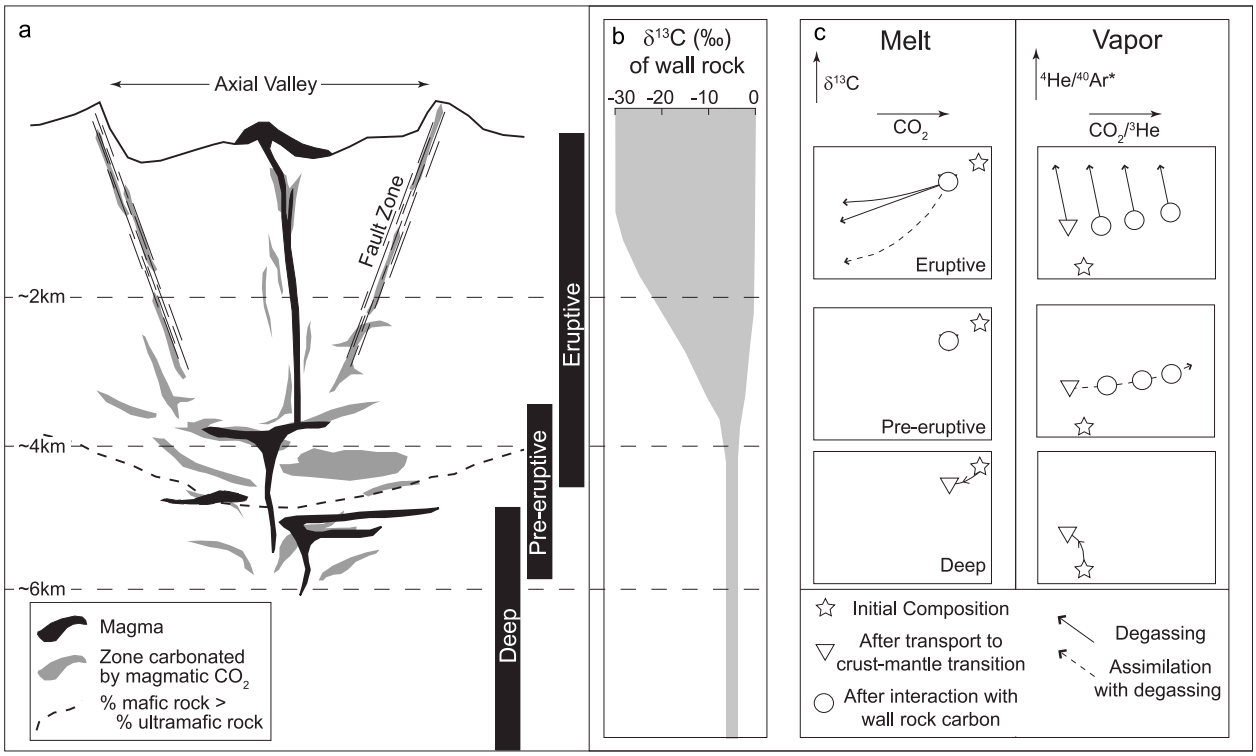

Figure 9. Schematic illustration of the magmatic plumbing beneath a slow spreading ridge segment and resulting degassing. (a) The likely extents of the three degassing stages identified from Southern Mariana Trough (SMT) glasses. (b) The extent of $\delta^{13}C$ heterogeneity in the crust and shallow mantle. Values are restricted in the deeper crust, where a flux of mantle carbon dominates. At shallower levels higher $\delta^{13}C$ values reflect hydrothermal carbonate derived from CO_2 saturated marine water, while lower $\delta^{13}C$ values reflect decomposition of magmatic CO_2 and the presence of organic carbon [*Alt and Teagle*, 1999; *Kelley and Früh-Green*, 2001; *Alt*, 2003]. (c) A schematic illustration of the evolution of dissolved CO_2 and CO_2-He-Ar in the vapor phase of SMT magma. At depth gas is lost by batch equilibrium degassing from an initial composition (star) until it ponds in the crust-mantle transition zone (inverted triangle). Some of this CO_2 causes carbonation of mantle and deep crustal rocks. During preeruptive storage the magma degasses due to crystallization, and the vapor phase acquires a range of $CO_2/^3He$ through interaction with carbonated wall rock (circles). Magma is then erupted onto the seafloor and loses gas by batch or fractional equilibrium degassing. Interaction with the crust during eruption is restricted in the Southern Mariana Trough.

that it is possible to see through these effects to melt-vapor partitioning at deeper levels [*Shaw et al.*, 2004, 2008; *Macpherson et al.*, 2005a; *Aiuppa et al.*, 2007; *Barsanti et al.*, 2009; *Collins et al.*, 2009; *Blundy et al.* 2010]. The SMT data also indicate that there may be challenges in reconciling behavior at deep levels between suites generated in different settings. For example, the early fractionation of CO_2, He and Ar into the vapor phase in the SMT suite is aided by the high water content of the melts. As a result, at any given pressure, SMT melt will have lost a larger fraction of its dissolved CO_2, He and Ar than dry magma with similar initial contents of these low-solubility species. Similarly, initial degassing of wet SMT melt will occur at greater depth than dry magma such that CO_2 fluxing of the shallow mantle and deep crust may occur over a greater depth interval in arc and back-arc settings than is this case at mid-ocean ridges. The influence of water upon degassing behavior will also be apparent at ocean islands and other sites of hydrous magmatism. Thus, there may be less opportunity to develop carbonated zones in the deep crust and shallow mantle where magma is water poor because the onset of degassing is likely to occur only at relatively shallow levels.

6. Volatile Subduction

[55] Subduction provides a mechanism to transport surface volatiles to the Earth's interior. As such, it has the potential to influence the composition, rheology and melting behavior of the mantle. Constraining the fluxes of volatile elements in

subduction zones is complicated by their extreme mobility, the diversity of sources that may contribute to the integrated flux measured at any single location and uncertainties in the integrity of samples provided by volcanic gases and rocks. This study has constrained a detailed history for degassing of SMT magma, which provides the opportunity to assess the extent to which volatile components are recycled through the Mariana Trough back arc.

6.1. Recycled Volatiles in the Mariana Trough Mantle

[56] After constraining the role of degassing and crustal contamination, there is little evidence for heterogeneity of carbon and helium in the source of SMT magmatism. As has been noted for other locations in the Mariana Trough, $^3He/^4He$ ratios of SMT magmatism are indistinguishable from MORB (Figure 4). Our investigation of degassing suggests that primitive values for $\delta^{13}C$ and $CO_2/^3He$ are also very similar to values for MORB (Figures 6 and 7). Thus, despite strong evidence for recycling of water (Figure 2) and incompatible trace elements in the N-SMT [*Gribble et al.*, 1996], there is no evidence that carbon or helium have been transferred from the subducted Pacific Plate into the SMT mantle.

[57] $^{40}Ar/^{36}Ar$ ratios are significantly lower than postulated MORB source values (≥40,000 [*Burnard et al.*, 1997]). However, the extensive degassing and contamination recognized from other parameters mean that $^{40}Ar/^{36}Ar$ will have been highly susceptible to modification during transport and so measured values are unlikely to be representative of the mantle source. We cannot exclude the possibility that $^{40}Ar/^{36}Ar$ ratios of primary SMT magma were different to MORB but we find no evidence to support this possibility. The inferred MORB-like $^4He/^{40}Ar^*$ and $CO_2/^{40}Ar^*$ ratios (Figures 5 and 7) lead us to infer that, like carbon and He, there is a negligible flux of recycled, subducted Ar contaminating the source of SMT magmatism.

[58] *Sano et al.* [1998] studied CO_2 and noble gases in Northern Mariana Trough glasses. They found no evidence for a recycled contribution at 18°N where two samples have MORB-like $^3He/^4He$, $\delta^{13}C$ and $CO_2/^3He$ values (Figure 10). However, they postulated that higher $\delta^{13}C$ and $CO_2/^3He$ values at 20°N indicated a mantle source containing subducted marine limestone. Using the model of *Sano and Marty* [1995], of simple mixing between three carbon end-members (mantle, subducted limestone and subducted organic sediment), suggests that the 20°N mantle would require ~50% of the CO_2 to be derived from subducted carbonates (Figure 10a). *Sano et al.* [1998] recognized that this simple mixing did not account for the effects of magma degassing. They corrected both $\delta^{13}C$ and $CO_2/^3He$ for the effects of a single stage of degassing, after which the amount of recycled, high-$\delta^{13}C$, marine limestone-derived CO_2 in the Northern Mariana mantle was revised to ~30%.

[59] Applying the *Sano and Marty* [1995] mixing model to the SMT data would lead to the conclusion that there had been substantial amounts of recycling of both marine limestone and organic sediment, with DS86-TYPE6 representing fluxes of >50% limestone and >25% organic carbon. However, section 5 demonstrates that the SMT variation can be accounted for through a three-stage degassing model from a MORB-like precursor (Figure 10b). Whereas the elevated $\delta^{13}C$ values of 20°N samples cannot be generated with exactly the same history as advocated for the SMT, the 20°N data can still be explained within the model illustrated in Figure 9. Shallow parts of oceanic crust sequences can contain substantial amounts of marine carbonate introduced by hydrothermal activity. Figure 10b demonstrates that 18°N magma can yield the 20°N characteristics through only ~5% degassing accompanied by assimilation of crust with dominantly marine $\delta^{13}C$ of 0‰ and containing 1.8 wt % CO_2 (mean of upper crust estimates by *Staudigel et al.* [1995] and *Alt and Teagle* [1999]). Contamination at shallower crustal levels in the northern Mariana Trough may be favored because seafloor spreading is less well established and rifting of older, and so potentially more carbonated, crust accommodates much of the back-arc extension [*Gribble et al.*, 1998]. Thus, we conclude that it is possible to generate all of the $\delta^{13}C$ and $CO_2/^3He$ heterogeneity observed in Mariana Trough basalts from starting compositions that are indistinguishable from MORB.

6.2. Implications for Recycling of Subducted Volatiles

[60] Estimating volatile fluxes through subduction zones presents many challenges [*Jambon*, 1994; *Hilton et al.*, 2002]. Significant advances have been made in understanding water due to its high solubility in basaltic melt, which means that near-primary H_2O concentrations can be observed in melt inclusions and/or be reconstructed for glasses then compared with lithophile elements to determine melting conditions and recycled fluxes [*Stolper and Newman*, 1994; *Wallace*, 2005; *Kelley et al.*, 2006, 2010; *Shaw et al.*, 2008; *Plank et al.*, 2009]. The

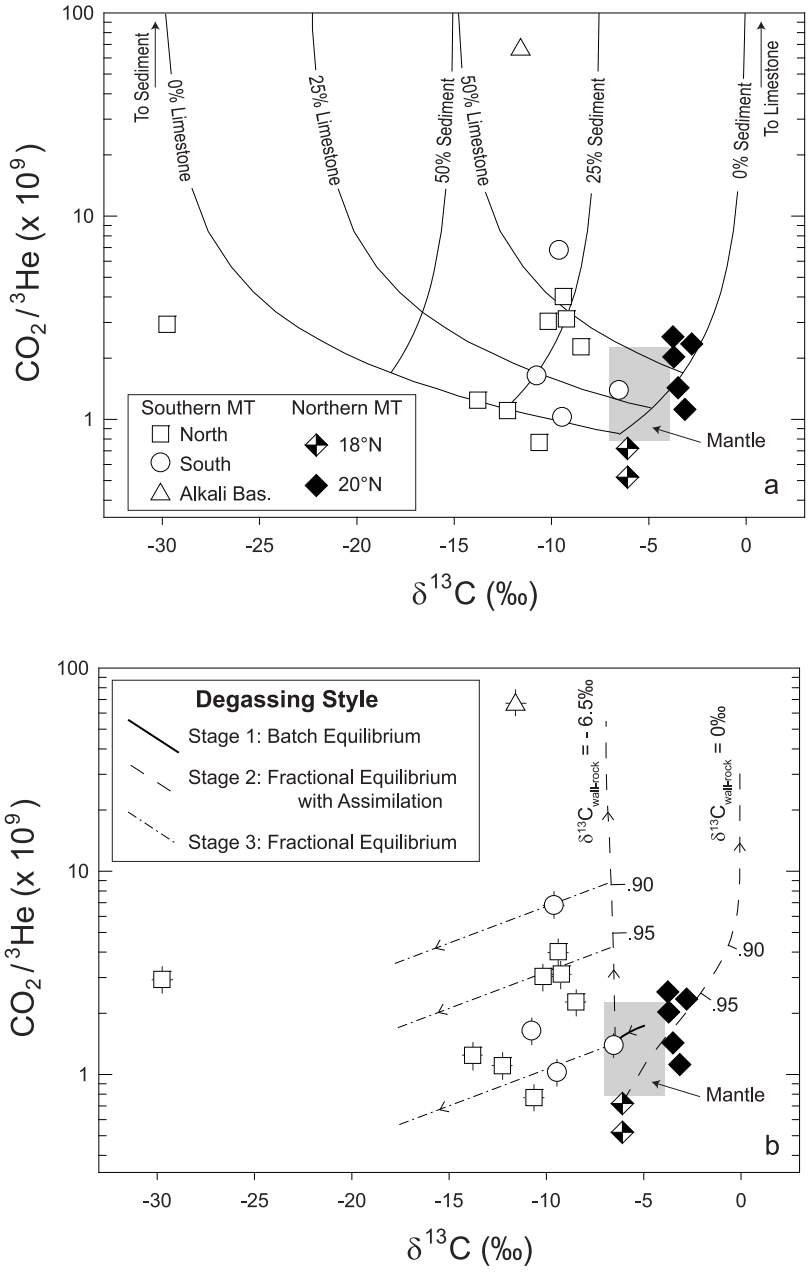

Figure 10. $CO_2/^3He$ versus $\delta^{13}C$ in vesicle gas from Mariana Trough basaltic glasses. Southern Mariana Trough (SMT) glasses from this work and Northern Mariana Trough glasses from *Sano et al.* [1998]. Shaded gray box represents the range estimated for the upper mantle source of MORB. (a) Solid lines illustrate three-component mixing model of *Sano and Marty* [1995] in which the composition of volcanic gas is resolved into mantle, limestone, and (organic-rich) sediment compositions. Each line represents a constant contribution from one of these components. See text for details. (b) Lines represent degassing stages identified in this work. The models fitted to the SMT data are those described in Figure 7. A fractional degassing with assimilation model is also shown for basalt from 18°N in the Northern Mariana Trough that interacts with crust containing 1.8 wt % CO_2 with $\delta^{13}C$ of 0‰ [*Staudigel et al.*, 1995; *Alt and Teagle*, 1999]. Tick marks on the fractional equilibrium degassing with assimilation curves represent the fraction of vapor retained during that stage of degassing.

low solubility of CO_2 in basaltic melt places greater obstacles in the way of using this approach to determine the primary characteristics of CO_2 in arc and back-arc magmatism.

[61] We have integrated information from dissolved and vapor components in SMT glasses to demonstrate that degassing and contamination can generate diverse volatile characteristics in back-arc

magmatism. This leads us to conclude that SMT magmatism contains no carbon derived from the subducted Pacific Plate. Furthermore, extending the model to sites further north (Figure 10b) suggests that there is a negligible recycled carbon flux anywhere in the Mariana back-arc. This is consistent with carbonate stabilities determined for old, cold oceanic crust undergoing subduction [*Kerrick and Connelly*, 2001; *Dasgupta et al.*, 2004; *Gorman et al.*, 2006; *Keshav and Gudfinnsson*, 2010]. Since water and lithophile components are effectively transferred from the slab to the back-arc mantle [*Gribble et al.*, 1996], it is unlikely that the steep dip of the Pacific slab prevents CO_2 transfer into the mantle wedge. We conclude that the flux of water and fluid mobile elements into Southern Mariana Trough back-arc magmatism is not accompanied by a flux of carbon. This implies that devolatilization of a cold slab fractionates subducted carbon from subducted water.

7. Conclusions

[62] The combined CO_2-He-Ar abundance and isotopic data set demonstrates that volatile heterogeneity in Mariana Trough basaltic magma is developed almost entirely during magma transport through the mantle wedge and crust. Initial melts leave the mantle source from which they inherit a range of water concentrations that reflect variable recycling from the subducted slab. In contrast, inferred initial values for $^3He/^4He$, $\delta^{13}C$, $CO_2/^3He$, $^4He/^{40}Ar^*$ and $CO_2/^{40}Ar^*$ are indistinguishable from MORB. This implies that the carbon and noble gas budgets of Mariana back-arc magmatism are dominated by the mantle wedge, with negligible input from the subducted slab. In the Mariana system any carbon in the slab that passes the zone of arc front magmatism is returned to the deep mantle. Exsolution of CO_2 and noble gases from hydrous, back-arc basaltic magma begins during transport through the mantle and continues until eruption. This provides a constant flux of CO_2 that interacts with wall rock in the mantle and crust, and can be remobilized by, and incorporated into the vapor phase of, subsequent melt batches.

Acknowledgments

[63] This research was supported by start-up funds to D.R.H. from Scripps Institution of Oceanography and grants from NSF (EAR-9614347; OCE-0305248) to D.R.H. and from NERC (NER/M/S/2001/00099) to C.G.M. Martin Wahlen kindly allowed us access to his laboratory to conduct carbon isotope measurements, with which Bruce Deck assisted. Samples were provided by Peter Stoffers (Kiel).

References

Aiuppa, A., R. Moretti, C. Federico, G. Giudice, S. Gurrieri, M. Liuzzo, P. Papale, H. Shinohura, and M. Valenza (2007), Forecasting Etna eruptions by real-time observation of volcanic gas composition, *Geology*, *35*(12), 1115–1118, doi:10.1130/G24149A.1.

Alt, J. C. (2003), Stable isotopic composition of upper oceanic crust formed at a fast spreading ridge, ODP Site 801, *Geochem. Geophys. Geosyst.*, *4*(5), 8908, doi:10.1029/2002GC000400.

Alt, J. C., and D. A. H. Teagle (1999), The uptake of carbon during alteration of oceanic crust, *Geochim. Cosmochim. Acta*, *63*(10), 1527–1535, doi:10.1016/S0016-7037(99)00123-4.

Alt, J. C., W. C. Shanks, and M. C. Jackson (1993), Cycling of sulfur in subduction zones: The geochemistry of sulfur in the Mariana Island Arc and back-arc trough, *Earth Planet. Sci. Lett.*, *119*(4), 477–494, doi:10.1016/0012-821X(93)90057-G.

Bach, W., and F. Klein (2009), The petrology of seafloor rodingites: Insights from geochemical reaction path modelling, *Lithos*, *112*(1–2), 103–117, doi:10.1016/j.lithos.2008.10.022.

Barsanti, M., P. Papale, D. Barbato, R. Moretti, E. Boschi, E. Hauri, and A. Longo (2009), Heterogeneous large total CO_2 abundance in the shallow magmatic system of Kilauea volcano, Hawaii, *J. Geophys. Res.*, *114*, B12201, doi:10.1029/2008JB006187.

Bibee, L. D., G. G. Shor Jr., and R. S. Lu (1980), Inter-arc spreading in the Mariana Trough, *Mar. Geol.*, *35*(1–3), 183–197, doi:10.1016/0025-3227(80)90030-4.

Blundy, J., K. V. Cashman, A. Rust, and F. Witham (2010), A case for CO_2-rich arc magmas, *Earth Planet. Sci. Lett.*, *290*(3–4), 289–301, doi:10.1016/j.epsl.2009.12.013.

Bonatti, E., C. Emiliani, G. Ferrara, J. Honnorez, and H. Rydell (1974), Ultramafic-carbonate breccias from the equatorial Mid-Atlantic Ridge, *Mar. Geol.*, *16*(2), 83–102, doi:10.1016/0025-3227(74)90057-7.

Burnard, P. (2001), Correction for volatile fractionation in ascending magmas: Noble gas abundance in primary mantle melts, *Geochim. Cosmochim. Acta*, *65*(15), 2605–2614, doi:10.1016/S0016-7037(01)00605-6.

Burnard, P., D. Graham, and G. Turner (1997), Vesicle-specific noble gas analyses of "popping rock": Implications for primordial noble gasses in Earth, *Science*, *276*(5312), 568–571, doi:10.1126/science.276.5312.568.

Burnard, P., D. Graham, and G. Turner (2004), Fractionation of noble gases (He, Ar) during MORB mantle melting: A case study on the Southeast Indian Ridge, *Earth Planet. Sci. Lett.*, *227*(3–4), 457–472, doi:10.1016/j.epsl.2004.08.021.

Carroll, M. R., and J. D. Webster (1994), Solubilities of sulphur, noble gases, nitrogen, chlorine and fluorine in magmas, in *Volatiles in Magmas*, *Rev. in Mineral. and Geochem.*, vol. 30, edited by M. R. Carroll and J. R. Holloway, pp. 231–279, Mineral. Soc. of Am., Washington, D. C.

Cartigny, P., N. Jendrzejewski, F. Pineau, E. Petit, and M. Javoy (2001), Volatile (C, N, Ar) variability in MORB and the respective roles of mantle source heterogeneity and degassing: The case of the Southwest Indian Ridge, *Earth Planet.*

Sci. Lett., *194*(1–2), 241–257, doi:10.1016/S0012-821X(01)00540-4.

Clark, I. D., and J.-C. Fontes (1990), Paleoclimatic reconstruction in northern Oman based on carbonate from hyperalkaline groundwaters, *Quat. Res.*, *33*(3), 320–336, doi:10.1016/0033-5894(90)90059-T.

Collins, S. J., D. M. Pyle, and J. Maclennan (2009), Melt inclusions track pre-eruption storage and dehydration of magmas at Etna, *Geology*, *37*(6), 571–574, doi:10.1130/G30040A.1.

Dalton, J. A., and B. J. Wood (1993), The partitioning of Fe and Mg between olivine and carbonate and the stability of carbonate under mantle conditions, *Contrib. Mineral. Petrol.*, *114*(4), 501–509.

Dasgupta, R., M. M. Hirschmann, and A. C. Withers (2004), Deep global cycling of carbon constrained by the solidus of anhydrous, carbonated eclogite under upper mantle conditions, *Earth Planet. Sci. Lett.*, *227*(1–2), 73–85, doi:10.1016/j.epsl.2004.08.004.

Day, J. M. D., D. R. Hilton, D. G. Pearson, C. G. Macpherson, B. A. Kjarsgaard, and P. E. Janney (2005), Absence of a high time-integrated ^{3}He/(U+Th) source in the mantle beneath continents, *Geology*, *33*(9), 733–736, doi:10.1130/G21625.1.

Deines, P. (2002), The carbon isotope geochemistry of mantle xenoliths, *Earth Sci. Rev.*, *58*(3–4), 247–278.

Dixon, J. E., and E. M. Stolper (1995), An experimental study of water and carbon dioxide solubilities in mid-ocean ridge basaltic liquids. Part II: Applications to degassing, *J. Petrol.*, *36*(6), 1633–1646.

Dixon, J. E., L. Leist, C. Langmuir, and J.-G. Schilling (2002), Recycled dehydrated lithosphere observed in plume-influenced mid-ocean ridge basalt, *Nature*, *420*(6914), 385–389, doi:10.1038/nature01215.

Fine, G., and E. Stolper (1986), Dissolved carbon dioxide in basaltic glasses: Concentration and speciation, *Earth Planet. Sci. Lett.*, *76*(3–4), 263–278, doi:10.1016/0012-821X(86)90078-6.

Garcia, M. O., N. W. K. Liu, and D. W. Muenow (1979), Volatiles in submarine volcanic rocks from the Mariana Island arc and trough, *Geochim. Cosmochim. Acta*, *43*(3), 305–312, doi:10.1016/0016-7037(79)90196-0.

Gerlach, T. M., and B. E. Taylor (1990), Carbon isotope constraints on degassing of carbon dioxide from Kilauea volcano, *Geochim. Cosmochim. Acta*, *54*(7), 2051–2058, doi:10.1016/0016-7037(90)90270-U.

Gorman, P. J., D. M. Kerrick, and J. A. D. Connolly (2006), Modeling open system metamorphic decarbonation of subducting slabs, *Geochem. Geophys. Geosyst.*, *7*, Q04007, doi:10.1029/2005GC001125.

Graham, D. W. (2002), Noble gas isotope geochemistry of mid-ocean ridge and ocean island basalts: Characterization of mantle source reservoirs, in *Noble Gases in Geochemistry and Cosmochemistry*, *Rev. in Mineral. and Geochem.*, vol. 47, edited by D. P. Porcelli, C. J. Ballentine, and R. Wieler, pp. 247–317, Mineral. Soc. of Am., Washington, D. C.

Gribble, R. F., R. J. Stern, S. H. Bloomer, D. Stuben, T. O'Hearn, and S. Newman (1996), MORB mantle and subduction components interact to generate basalts in the southern Mariana Trough back-arc basin, *Geochim. Cosmochim. Acta*, *60*(12), 2153–2166, doi:10.1016/0016-7037(96)00078-6.

Gribble, R. F., R. J. Stern, S. Newman, S. H. Bloomer, and T. O'Hearn (1998), Chemical and isotopic composition of lavas from the Northern Mariana Trough: Implications for magmagenesis in back-arc basins, *J. Petrol.*, *39*(1), 125–154, doi:10.1093/petrology/39.1.125.

Hammerschmidt, K. (1986), ^{40}Ar-^{39}Ar dating of young samples, in *Dating Young Sediments*, edited by A. J. Hurford, E. Jager, and J. A. M. Ten Cate, pp. 339–357, CCOP Tech. Secr., Bangkok, Thailand.

Hayes, J. F., and J. R. Waldbauer (2006), The carbon cycle and associated redox processes through time, *Philos. Trans. R. Soc. B*, *361*, 931–950, doi:10.1098/rstb.2006.1840.

Heber, V. S., R. A. Brooker, S. P. Kelley, and B. J. Wood (2007), Crystal-melt partitioning of noble gases (helium, neon, argon, krypton, and xenon) for olivine and clinopyroxene, *Geochim. Cosmochim. Acta*, *71*(4), 1041–1061, doi:10.1016/j.gca.2006.11.010.

Hilton, D. R., K. Hammerschmidt, G. Loock, and H. Friedrichsen (1993), Helium and argon isotope systematics of the central Lau Basin and Valu Fa Ridge: Evidence of crust/mantle interactions in a backarc basin, *Geochim. Cosmochim. Acta*, *57*(12), 2819–2841, doi:10.1016/0016-7037(93)90392-A.

Hilton, D. R., J. Barling, and G. E. Wheller (1995), Effects of shallow-level contamination on the helium isotope systematics of ocean-island lavas, *Nature*, *373*(6512), 330–333, doi:10.1038/373330a0.

Hilton, D. R., G. M. McMurtry, and F. Goff (1998), Large variations in vent fluid CO_2/^{3}He ratios signal rapid changes in magma chemistry at Loihi seamount, Hawaii, *Nature*, *396*(6709), 359–362, doi:10.1038/24603.

Hilton, D. R., T. P. Fischer, and B. Marty (2002), Noble gases and volatile recycling at subduction zones, in *Noble Gases in Geochemistry and Cosmochemistry*, *Rev. in Mineral. and Geochem.*, vol. 47, edited by D. P. Porcelli, C. J. Ballentine, and R. Wieler, pp. 319–370, Mineral. Soc. of Am., Washington, D. C.

Hilton, D. R., T. P. Fischer, A. J. S. McGonigle, and J. M. de Moor (2007), Variable SO_2 emission rates for Anatahan volcano, the Commonwealth of the Northern Mariana Islands: Implications for deriving arc-wide volatile fluxes from erupting volcanoes, *Geophys. Res. Lett.*, *34*, L14315, doi:10.1029/2007GL030405.

Hirschmann, M. M., and R. Dasgupta (2009), The H/C ratios of Earth's near-surface and deep reservoirs, and consequences for deep Earth volatiles, *Chem. Geol.*, *262*(1–2), 4–16, doi:10.1016/j.chemgeo.2009.02.008.

Ikeda, Y., N. Keisuke, R. J. Stern, M. Yuasa, and S. Newman (1998), Noble gases in pillow basalt glasses from the northern Mariana Trough back-arc basin, *Isl. Arc*, *7*(3), 471–478, doi:10.1111/j.1440-1738.1998.00204.x.

Jambon, A. (1994), Earth degassing and large-scale geochemical cycling of volatile elements, in *Volatiles in Magmas*, *Rev. in Mineral. and Geochem.*, vol. 30, edited by M. J. Carroll and J. R. Holloway, pp. 479–517, Mineral. Soc. of Am, Washington, D. C.

Jambon, A., H. W. Weber, and O. Braun (1986), Solubility of He, Ne, Ar, Kr and Xe in a basalt melt in the range 1250–1600°C. Geochemical implications, *Geochim. Cosmochim. Acta*, *50*(3), 401–408, doi:10.1016/0016-7037(86)90193-6.

Kelemen, P. B., and J. Matter (2008), In situ carbonation of peridotite for CO_2 storage, *Proc. Natl. Acad. Sci. U. S. A.*, *105*(45), 17,295–17,300, doi:10.1073/pnas.0805794105.

Kelley, D. S., and G. L. Früh-Green (2001), Volatile lines of descent in submarine plutonic environments: Insights from stable isotope and fluid-inclusion analyses, *Geochim. Cosmochim. Acta*, *65*(19), 3325–3346, doi:10.1016/S0016-7037(01)00667-6.

Kelley, K. A., T. Plank, T. L. Grove, E. M. Stolper, S. Newman, and E. Hauri (2006), Mantle melting as a function of water

content beneath back-arc basins, *J. Geophys. Res.*, *111*, B09208, doi:10.1029/2005JB003732.

Kelley, K. A., T. Plank, S. Newman, E. M. Stolper, T. L. Grove, S. Parman, and E. Hauri (2010), Mantle melting as a function of water content beneath the Mariana Arc, *J. Petrol.*, *51*(8), 1711–1738, doi:10.1093/petrology/egq036.

Kerrick, D. M., and J. A. D. Connelly (2001), Metamorphic devolatilization of subducted oceanic metabasalts: Implications for seismicity, arc magmatism and volatile recycling, *Earth Planet. Sci. Lett.*, *189*(1–2), 19–29, doi:10.1016/S0012-821X(01)00347-8.

Keshav, S., and G. H. Gudfinnsson (2010), Experimentally dictated stability of carbonated oceanic crust to moderately great depths in the Earth: Results from the solidus determination in the system CaO-MgO-Al_2O_3-SiO_2-CO_2, *J. Geophys. Res.*, *115*, B05205, doi:10.1029/2009JB006457.

Kitada, K., N. Seama, T. Yamazaki, Y. Nogi, and K. Suyehiro (2006), Distinct regional differences in crustal thickness along the axis of the Mariana Trough, inferred from gravity anomalies, *Geochem. Geophys. Geosyst.*, *7*, Q04011, doi:10.1029/2005GC001119.

Luth, R. W. (1999), Carbon and carbonate in the mantle, in *Mantle Petrology: Field Observations and High Pressure Experimentation: A Tribute to Francis R. (Joe) Boyd*, edited by Y. Fei, C. M. Bertka, and B. O. Mysen, Spec. Publ. Geochem. Soc., 6, 297–316.

Macpherson, C. G., and D. P. Mattey (1994), Carbon isotope variations of CO_2 in Lau Basin basalts and ferrobasalts, *Earth Planet. Sci. Lett.*, *121*(3–4), 263–276, doi:10.1016/0012-821X(94)90072-8.

Macpherson, C. G., and D. P. Mattey (1998), Oxygen isotope variations in Lau Basin lavas, *Chem. Geol.*, *144*(3–4), 177–194, doi:10.1016/S0009-2541(97)00130-7.

Macpherson, C. G., D. R. Hilton, J. M. Sinton, R. J. Poreda, and H. Craig (1998), High $^3He/^4He$ ratios in the Manus backarc basin: Implications for mantle mixing and the origin of plumes in the western Pacific Ocean, *Geology*, *26*(11), 1007–1010, doi:10.1130/0091-7613(1998)026<1007:HHRIT>2.3.CO;2.

Macpherson, C. G., D. R. Hilton, S. Newman, and D. P. Mattey (1999), CO_2, $^{13}C/^{12}C$ and H_2O variability in natural basaltic glasses: A study comparing stepped heating and FTIR spectroscopic techniques, *Geochim. Cosmochim. Acta*, *63*(11–12), 1805–1813, doi:10.1016/S0016-7037(99)00124-6.

Macpherson, C. G., D. R. Hilton, D. P. Mattey, and J. M. Sinton (2000), Evidence for an ^{18}O-depleted mantle plume from contrasting $^{18}O/^{16}O$ ratios of back-arc lavas from the Manus Basin and Mariana Trough, *Earth Planet. Sci. Lett.*, *176*(2), 171–183, doi:10.1016/S0012-821X(00)00002-9.

Macpherson, C. G., D. R. Hilton, D. F. Mertz, and T. J. Dunai (2005a), Sources, degassing and contamination of CO_2, H_2O, He, Ne and Ar in basaltic glasses from Kolbeinsey Ridge, North Atlantic, *Geochim. Cosmochim. Acta*, *69*(24), 5729–5746, doi:10.1016/j.gca.2005.07.015.

Macpherson, C. G., D. R. Hilton, J. M. D. Day, D. Lowry, and K. Grönvold (2005b), High-$^3He/^4He$, depleted mantle and low-$\delta^{18}O$, recycled oceanic lithosphere in the source of central Iceland magmatism, *Earth Planet. Sci. Lett.*, *233*(3–4), 411–427, doi:10.1016/j.epsl.2005.02.037.

Marty, B., and L. Zimmermann (1999), Volatiles (He, C, N, Ar) in mid-ocean ridge basalts: Assessment of shallow-level fractionation and characterization of source composition, *Geochim. Cosmochim. Acta*, *63*(21), 3619–3633, doi:10.1016/S0016-7037(99)00169-6.

Marty, B., Y. Sano, and C. France-Lanord (2001), Water-saturated oceanic lavas from the Manus Basin: Volatile behaviour during assimilation-fractional crystallization-degassing (AFCD), *J. Volcanol. Geotherm. Res.*, *108*(1–4), 1–10, doi:10.1016/S0377-0273(00)00275-4.

Mattey, D. P., R. H. Carr, I. P. Wright, and C. T. Pillinger (1984), Carbon isotopes in submarine basalts, *Earth Planet. Sci. Lett.*, *70*(2), 196–206, doi:10.1016/0012-821X(84)90005-0.

Michael, P. (1995), Regionally distinctive sources of depleted MORB: Evidence from trace elements and H_2O, *Earth Planet. Sci. Lett.*, *131*(3–4), 301–320, doi:10.1016/0012-821X(95)00023-6.

Moreira, M., and P. Sarda (2000), Noble gas constraints on degassing processes, *Earth Planet. Sci. Lett.*, *176*(3–4), 375–386, doi:10.1016/S0012-821X(00)00010-8.

Newman, S., E. Stolper, and R. Stern (2000), H_2O and CO_2 in magmas from the Mariana arc and back arc systems, *Geochem. Geophys. Geosyst.*, *1*(5), 1013, doi:10.1029/1999GC000027.

Nishio, Y., S. Sasaki, T. Gamo, H. Hiyagon, and Y. Sano (1998), Carbon and helium isotope systematics of North Fiji Basin basalt glasses: Carbon geochemical cycle in the subduction zone, *Earth Planet. Sci. Lett.*, *154*(1–4), 127–138, doi:10.1016/S0012-821X(97)00187-8.

Paonita, A., G. Gigli, D. Gozzi, P. M. Nuccio, and R. Trigila (2000), Investigation of the He solubility in H_2O-CO_2 bearing silicate liquids at moderate pressure: A new experimental method, *Earth Planet. Sci. Lett.*, *181*(4), 595–604, doi:10.1016/S0012-821X(00)00215-6.

Pearce, J. A., R. J. Stern, S. H. Bloomer, and P. Fryer (2005), Geochemical mapping of the Mariana arc-basin system: Implications for the nature and distribution of subduction components, *Geochem. Geophys. Geosyst.*, *6*, Q07006, doi:10.1029/2004GC000895.

Pineau, F., and M. Javoy (1983), Carbon isotopes and concentrations in mid-ocean ridge basalts, *Earth Planet. Sci. Lett.*, *62*(2), 239–257, doi:10.1016/0012-821X(83)90087-0.

Pineau, F., and M. Javoy (1994), Strong degassing at ridge crests: The behaviour of dissolved carbon and water in basalt glasses at 14°N, Mid-Atlantic Ridge, *Earth Planet. Sci. Lett.*, *123*(1–3), 179–198, doi:10.1016/0012-821X(94)90266-6.

Plank, T., L. B. Cooper, and C. E. Manning (2009), Emerging geothermometers for estimating slab surface temperatures, *Nat. Geosci.*, *2*(9), 611–615, doi:10.1038/ngeo614.

Poreda, R. (1985), Helium-3 and deuterium in back-arc basalts: Lau Basin and the Mariana Trough, *Earth Planet. Sci. Lett.*, *73*(2–4), 244–254, doi:10.1016/0012-821X(85)90073-1.

Poreda, R., and H. Craig (1989), Helium isotope ratios in circum-Pacific volcanic arcs, *Nature*, *338*(6215), 473–478, doi:10.1038/338473a0.

Python, M., G. Ceuleneer, Y. Ishida, J.-A. Barrat, and S. Arai (2007), Oman diopsidites: A new lithology diagnostic of very high temperature hydrothermal circulation in mantle peridotite below oceanic spreading centres, *Earth Planet. Sci. Lett.*, *255*(3–4), 289–305, doi:10.1016/j.epsl.2006.12.030.

Resing, J. A., J. E. Lupton, R. A. Feely, and M. D. Lilley (2004), CO_2 and ^3He in hydrothermal plumes: Implications for mid-ocean ridge CO_2 flux, *Earth Planet. Sci. Lett.*, *226*(3–4), 449–464, doi:10.1016/j.epsl.2004.07.028.

Ridgwell, A., and R. E. Zeebe (2005), The role of the global carbonate cycle in the regulation and evolution of the Earth system, *Earth Planet. Sci. Lett.*, *234*, 299–315, doi:10.1016/j.epsl.2005.03.006.

Sano, Y., and B. Marty (1995), Origin of carbon in fumarolic gas from island arcs, *Chem. Geol.*, *119*(1–4), 265–274, doi:10.1016/0009-2541(94)00097-R.

Sano, Y., Y. Nishio, T. Gamo, A. Jambon, and B. Marty (1998), Noble gas and carbon isotopes in Mariana Trough basalt glasses, *Appl. Geochem.*, *13*(4), 441–449, doi:10.1016/S0883-2927(97)00090-5.

Scheele, N., and J. Hoefs (1992), Carbon isotope fractionation between calcite, graphite and CO_2: An experimental study, *Contrib. Mineral. Petrol.*, *112*(1), 35–45, doi:10.1007/BF00310954.

Shaw, A. M., D. R. Hilton, C. G. Macpherson, and J. M. Sinton (2004), The CO_2-He-Ar-H_2O systematics of the Manus back-arc basin: Resolving source composition from degassing and contamination effects, *Geochim. Cosmochim. Acta*, *68*(8), 1837–1855, doi:10.1016/j.gca.2003.10.015.

Shaw, A. M., E. H. Hauri, T. P. Fischer, D. R. Hilton, and K. A. Kelley (2008), Hydrogen isotopes in Mariana arc melt inclusions: Implications for subduction dehydration and the deep-Earth water cycle, *Earth Planet. Sci. Lett.*, *275*(1–2), 138–145, doi:10.1016/j.epsl.2008.08.015.

Spilliaert, N., P. Allard, N. Métrich, and A. V. Sobolev (2006), Melt inclusion record of the conditions of ascent, degassing, and extrusion of volatile-rich alkali basalt during the powerful 2002 flank eruption of Etna (Italy), *J. Geophys. Res.*, *111*, B04203, doi:10.1029/2005JB003934.

Staudigel, H., G. R. Davies, S. R. Hart, K. M. Marchant, and M. Smith (1995), Large scale isotopic Sr, Nd and O isotopic anatomy of altered oceanic crust: DSDP/ODP sites 417/418, *Earth Planet. Sci. Lett.*, *130*(1–4), 169–185, doi:10.1016/0012-821X(94)00263-X.

Stolper, E., and S. Newman (1994), The role of water in the petrogenesis of Mariana trough magmas, *Earth Planet. Sci. Lett.*, *121*(3–4), 293–325, doi:10.1016/0012-821X(94)90074-4.

Stüben, D., T. Neuman, N.-E. Taibi, and G. P. Galsby (1998), Segmentation of the southern Mariana back-arc spreading centre, *Isl. Arc*, *7*(3), 513–524, doi:10.1111/j.1440-1738.1998.00207.x.

van Soest, M. C., D. R. Hilton, C. G. Macpherson, and D. P. Mattey (2002), Resolving sediment subduction and crustal contamination in the Lesser Antilles island arc: A combined He-O-Sr isotope approach, *J. Petrol.*, *43*(1), 143–170, doi:10.1093/petrology/43.1.143.

Wallace, P. J. (2005), Volatiles in subduction zone magmas: Concentrations and fluxes based on melt inclusion and volcanic gas data, *J. Volcanol. Geotherm. Res.*, *140*(1–3), 217–240, doi:10.1016/j.jvolgeores.2004.07.023.

Wyllie, P. J. (1977) Mantle fluid compositions buffered by carbonates in peridotite-CO_2-H_2O, *J. Geol.*, *85*(2), 187–207.